International Journal of Mechanical Sciences 270 (2024) 109097

Contents lists available at ScienceDirect

International Journal of Mechanical Sciences

journal homepage: www.elsevier.com/locate/ijmecsci

A wearable hydraulic shock absorber with efficient energy dissipation

Nicholas J. Cecchi [b], Yuzhe Liu [a,b,*], Ramanand V. Vegesna [c], Xianghao Zhan [b], Weiguang Yang [b,d], Leslie Anasu Espinoza Campomanes [b], Gerald A. Grant [e,f,g], David B. Camarillo [h]

[a] School of Biological Science and Medical Engineering, Beihang University, Beijing 100191, China
[b] Department of Bioengineering, Stanford University, Stanford, CA 94305, USA
[c] Department of Biomedical Engineering, University of Southern California, Los Angeles, CA 90089, USA
[d] Department of Pediatrics, Stanford University, Stanford, CA 94305, USA
[e] Department of Neurosurgery, Stanford University, Stanford, CA 94305, USA
[f] Department of Neurology, Stanford University, Stanford, CA 94305, USA
[g] Department of Neurosurgery, Duke University, NC 27710, USA
[h] Savior Brain, Inc., Vienna, VA 22180, USA

ARTICLE INFO

Keywords:
Hydraulics
Liquid
Helmet
Energy absorption
Brain injury
Personal protective equipment

ABSTRACT

Advances in shock absorber technology are often translated to wearable personal protective equipment (PPE) to protect humans from impact-related injuries. However, the effectiveness of PPE is limited by factors such as the tolerable size and weight of the PPE device and the environmental conditions in which the PPE will be used. In this study, we leveraged the energy dissipation of fluid flow using soft structures to prototype a novel, wearable hydraulic shock absorber — the Soft Hydraulic Shock. The Soft Hydraulic Shock achieved an efficient energy absorption ratio of 100 % across a range of impact loading conditions due to its fluid-based mechanism of energy absorption. In comparison, five state-of-the-art shock-absorbing technologies with similar dimensions and weights used in American football helmets were found to have average energy absorption ratios ranging from 74.0 % to 90.0 %, on average. Furthermore, the Soft Hydraulic Shock maintained a stable energy dissipation across a wide range of temperatures (-18 °C, 19.5 °C, 50 °C), while the energy dissipation of other shock absorbing technologies varied up to 20 % across these temperatures. Analyses of the behavior of the Soft Hydraulic Shock with different design parameters and impact loadings were further explored with a validated finite element model of the device. Finally, the Soft Hydraulic Shock demonstrated the ability to significantly mitigate brain injury risk (average 23.9 % reduction in Head Acceleration Response Metric) when implemented into a full helmet system. The results of this study demonstrate the promise of wearable hydraulic shock absorbers and provide a platform for further optimizing their performance.

1. Introduction

A variety of settings, such as automotive accidents, military combat, falls, and contact sports, present a risk of exposing the human body to impacts that can lead to serious injury. Wearable personal protective equipment (PPE) can play a key role in mitigating the risk of injury in these cases. The ability of wearable PPE to attenuate impacts mainly depends upon the shock-absorbing technology utilized. However, several constraints exist for shock absorbers implemented into wearable PPE. First, there is a limit to how large PPE products can be without hindering the abilities and performance of the wearer, so a shock absorber must be compact, its size usually limited to a few centimeters in height. The overall mass of the PPE device must also be tolerable for the wearers, which limits the total weight of the installed shock absorbers. Furthermore, wearers often expect their PPE to yield reliable protection in various environmental conditions (e.g., temperature and humidity), so the impact responses of the energy-absorbing components within a PPE product need to be consistent across different application environments.

Helmets are a common form of wearable PPE used for impact protection and have been adopted for use in many human activities to reduce the risk of head and brain injuries [1]. The direct force from an

* Corresponding author at: School of Biological Science and Medical Engineering, Beihang University, Beijing 100083, China.
E-mail address: yuzheliu@buaa.edu.cn (Y. Liu).

https://doi.org/10.1016/j.ijmecsci.2024.109097
Received 8 November 2023; Received in revised form 10 February 2024; Accepted 10 February 2024
Available online 10 February 2024

impact to the head can result in skull fracture [2], and the acceleration of the head following an impact yields an inertial loading on the brain that can trigger the pathology leading to a traumatic brain injury (TBI) [3]. TBI affects approximately 55 million individuals annually across the world [4] and remains a persisting problem in many helmeted settings [1,5,6]. A potential reason for this is the complexity and nonlinearity of head impacts: first, the brain is injured by tissue deformation [7,8], but the quantitative relationship between the strain of the brain tissue and injury outcome remains elusive [9]; second, because of the skull's structure and the viscoelasticity of brain tissue, brain strain is in a highly nonlinear relationship with the kinematics of the head after sustaining an impact [10,11]; third, the rotational acceleration of the head, believed to be a primary mechanism of inducing brain strain [12], is decided by both the impact force and the helmet-head-neck system, which involves the contact between the helmet and the impact source as well as the neck's rotational response [13,14]. Because most helmets have not yet been tested and optimized to reduce brain strain [15], the current protection offered by helmets may not be adequate to prevent injury.

A wide variety of shock-absorbing technologies have been developed over the past several decades and implemented into helmets in an effort to reduce TBI risk. Foams have traditionally been used as helmet shock absorbers. Common examples of energy-absorbing foams in helmets include expanded polystyrene [16], expanded polypropylene [17], and polyurethane [18] padding materials of a variety of thicknesses and densities. However, many new foams and other impact-attenuating technologies and structures are rapidly being developed to improve the protection offered by helmets [19]. For example, additively manufactured lattices [20], honeycomb structures [21,22], and foams with fluid channels [23] have all been studied for use in helmets. Especially in American football, a contact sport with a relatively high frequency of severe head impacts [24], helmets also feature advanced shock absorbers that utilize a wide variety of mechanisms for dissipating impact energy [25–28]. Only in recent years, helmets for sports and recreation have been examined in research studies to minimize the six-degree-of-freedom kinematics of the head and the strain of the brain tissue resulting from impacts [29–31]. Laboratory impact test protocols have been developed to evaluate helmets for their ability to mitigate the risk of concussion, a mild form of TBI [32–34]. Analytical models of the helmet-head system have also been built to evaluate and optimize the protection offered by helmets [35], and modal analyses have been applied to investigate the brain during helmeted impacts [36]. Head impacts occurring in real incidents have also been reconstructed using extensive laboratory reconstructions [37] and simulation [38] to evaluate helmet performance.

Many different industries outside of PPE share the common need of absorbing undesired kinetic energy from impacts. In the field of impact engineering, shock absorbers utilize a variety of energy-absorbing mechanisms. Approaches including the crushing of cellular material, lattices, and honeycomb structures [39–41], plasticity and cracking [42–45], and hydraulics [46,47] have been developed to dissipate the kinetic energy of impacts. Hydraulic shock absorbers are distinctly different from other mechanisms of energy absorption, as the kinetic energy is dissipated by the pressing of fluid through a small orifice and the reaction forces depend on the compressing velocity rather than the displacement of the shock absorber. Because of this, hydraulic shock absorbers act as a pure damping unit instead of an elastic unit and can adaptively dissipate energy in repeated impacts with a large range of impact velocities. Given this ability, hydraulic shock absorbers have been widely used in situations where repeated impacts may happen and rebounding is not desired (e.g., automotive suspension [46]). Contact sports helmets represent a promising application in which hydraulic shock absorbers could be used to advance the state of the art in mitigating impact energy. Athletes in contact sports can sustain many repeated impacts to the head, and these impacts may span a wide range of velocities depending on the sport in which they occur [48,49]. However, traditional hydraulic shock absorbers would not be suitable for implementation into helmets or other wearable PPE without significant redesign. Traditional hydraulic shock absorbers yield high forces at the beginning of an impact and then decrease in force rapidly in a square relationship with their compressing velocity, which limits their total energy absorption. Further, the rigid structures comprising their design limit their effective stroke to only half of their total height (i.e., when pressing a piston into a tube, the maximum stroke is shorter than the tube or the piston), which makes them inefficient in dissipating energy in certain applications, like helmets, where shock absorber height is a major design limitation [50]. The complicated structure and heavy weight of existing hydraulic shock absorbers also makes it difficult for this technology to be applied to wearable PPE. Finally, the fluid used within a wearable hydraulic shock absorber would need to be both biocompatible (in case it contacted the user) and capable of maintaining a consistent impact response across different environmental conditions.

In this study, we present the Soft Hydraulic Shock: a novel, compact, and wearable hydraulic shock absorber that dissipates impact energy by pressing fluid through orifices. We prototyped this technology with soft components, including high-strength fabrics and medical balloons, and its overall height and weight were kept close to the shock absorbers currently used in American football helmets. Compared with five state-of-the-art shock absorbers currently used in football helmets, the Soft Hydraulic Shock exhibited the most favorable values of energy absorption ratio, a metric that describes the ability of a shock absorber to dissipate impact energy. Furthermore, the variations of the energy absorption ratio across high, low, and ambient temperatures were also measured, and the Soft Hydraulic Shock was found to exhibit a favorably stable response across all three temperature conditions in comparison to the other tested shock absorbers. Then, we modeled the Soft Hydraulic Shock using finite element analysis (FEA) in order to calculate the internal fluid pressure and determine the influence of orifice area and impact loading on the technology's force attenuation capabilities. Finally, the Soft Hydraulic Shock significantly mitigated brain injury risk metrics in laboratory head impact tests, including when it was implemented into a full helmet system as a replacement for energy-absorbing comfort padding and as a shock absorber placed inside of a chinstrap. Overall, the results of this study demonstrate the adaptive ability of the Soft Hydraulic Shock to efficiently dissipate impact energy under a wide variety of loading conditions and support further development of hydraulic shock absorber technology in the context of wearable PPE.

The remainder of this paper is structured as follows: First, we introduce the physics of energy absorption in the Soft Hydraulic Shock and describe the materials and processes used for prototyping the device. Next, we present the drop test methodology utilized for impact testing. We then display a validated finite element (FE) model of the Soft Hydraulic Shock and introduce parametric analyses using this FE model. Finally, we showcase translation of the Soft Hydraulic Shock Absorber to head impact protection, including its performance when directly affixed to a test headform and when integrated into American football helmets. The Methods and Results sections are arranged in the same sequence as described above, and the Discussion section is arranged according to the presentation of the specific results shared.

2. Methods

The theoretical and practical design and testing of the Soft Hydraulic Shock in prototype and simulation form are described in this section. In the prototype, the Soft Hydraulic Shock was tested alongside five state-of-the-art helmet shock absorbers for its ability to dissipate impact energy with varying impact mass, impact speed, and environmental temperature. Using the experimental data, a finite element model of the Soft Hydraulic Shock was developed and validated, then used to further explore the effect of changing impact mass, impact speed, and design parameters on the impact response of the device. Finally, prototypes of

the Soft Hydraulic Shock are tested for their ability to reduce brain injury risk when implemented into a helmet system.

2.1. Design and prototype

The concept of fluid pressure change through an orifice has been used in hydraulic shock absorbers previously, in designs that consist of a piston and a tube made of metal [46]. Although hydraulic shock absorbers have been widely used in industries such as the automotive industry, their high mass and complicated structure limit their utility in weight-sensitive and space-sensitive applications, such as PPE, in particular, helmets. To reduce weight and maximize the stroke of a hydraulic shock absorber, we designed and prototyped the Soft Hydraulic Shock as shown in Fig. 1c–g: when an impact mass contacts the shock absorber (Fig. 1a), the fluid stored in a central balloon is forced to travel into elastic refill chambers through two orifice tubes on opposite sides of the balloon. Then, high pressure yielded by the orifices results in a high reaction force to decelerate the impact mass. Adopting the assumption that the liquid follows Bernoulli's equation, the reaction force of the Soft Hydraulic Shock is

$$F = \frac{A_C^3}{4A_O^2} \cdot \rho \cdot \frac{V_C^2}{2C_d^2}, \tag{1}$$

where F is the reaction force, A_C is the contact area between the impact mass and the shock absorber, V_C is the velocity of the impact mass, A_O is the orifice area, C_d is the discharge coefficient, and ρ is the density of the fluid. See the Supplementary Materials Section S1 for further details and derivation of this equation.

As an impact mass compresses the Soft Hydraulic Shock, the fluid held inside the shock is pushed through an orifice tube (Fig. 1a, b). According to Bernoulli's principle, the accelerated fluid velocity after the orifice generates an increasing pressure in the shock, which yields the reaction force to decelerate the impact mass. We prototyped the Soft Hydraulic Shock as shown in Fig. 1c, in which we used a medical balloon (Fig. 1g) to hold the fluid and a high-strength fabric (Fig. 1d) to avoid expansion of the shock itself. A fixed orifice was created with tubes (Fig. 1e) which connected the balloon to elastic refill chambers (Fig. 1f), which temporarily store the fluid passing through the orifice and push the fluid back into the balloon after an impact. To achieve a similar height to shock absorbers used in helmets, two assemblies shown in Fig. 1c were stacked together, forming the Soft Hydraulic Shock (SoftShox, Savior Brain, Inc; Vienna, VA).

In each stack of the Soft Hydraulic Shock, a medical balloon (Poba Medical; Flagstaff, AZ) (Fig. 1g) is used to store the fluid and is wrapped in an upper and lower layer of high-strength fabric (Dyneema, thickness=0.2 mm) that are sewn together in a circular pattern that surrounds the balloon (r_0=22 mm, Fig. 1d). Then, the two individual stacks are connected via stitching along a circle of smaller radius (r_s=15 mm, Fig. 1d). The surrounding fabric inflates when the inner balloon is filled with fluid (Fig. 1c). During an impact, the fabric is able to collapse, but rigidly constrains the local expansion of the balloon. As a result, all of the fluid flows through the orifices instead of causing local expansion of the balloon. Two rigid polyurethane tubes (inner diameter=4 mm, outer diameter=6 mm, length=37 mm) are adhered to the medical balloon and serve as the orifices for each stack (Fig. 1e), and two latex surgical tubes (inner diameter=4.6 mm, outer diameter=6.6 mm) function as elastic refill chambers (Fig. 1f). When the fluid enters these refill chambers, the latex tubes expand and subject low pressure on the fluid, forcing it back into the central balloon after the impact (Fig. 1b). Cable ties are used to constrain the orifice tube to the fabric and the refill chamber to the orifice tube, therefore sealing the refill chamber and strengthening the connection between the orifice tube and the refill chamber. Considering that helmet shock absorbers are meant to be used in different temperatures and should be safe for contact with human skin, propylene glycol was selected as the fluid for use due to its low freezing point (-59 °C) and biocompatibility. To achieve a shock absorber height similar to shock absorbers found in protective helmets, the Soft Hydraulic Shock is designed in a two-stack style (Fig. 1a and b). After final assembly, the height and mass of the Soft Hydraulic Shock were measured as 32 mm and 49.4 ± 0.9 g, respectively.

2.2. Shock absorber unit testing

In this study, the Soft Hydraulic Shock was tested by dropping an impact mass onto the shock absorbers from three different drop heights (corresponding to aimed impact speeds of 1.9, 2.5, and 3.2 m/s) and two

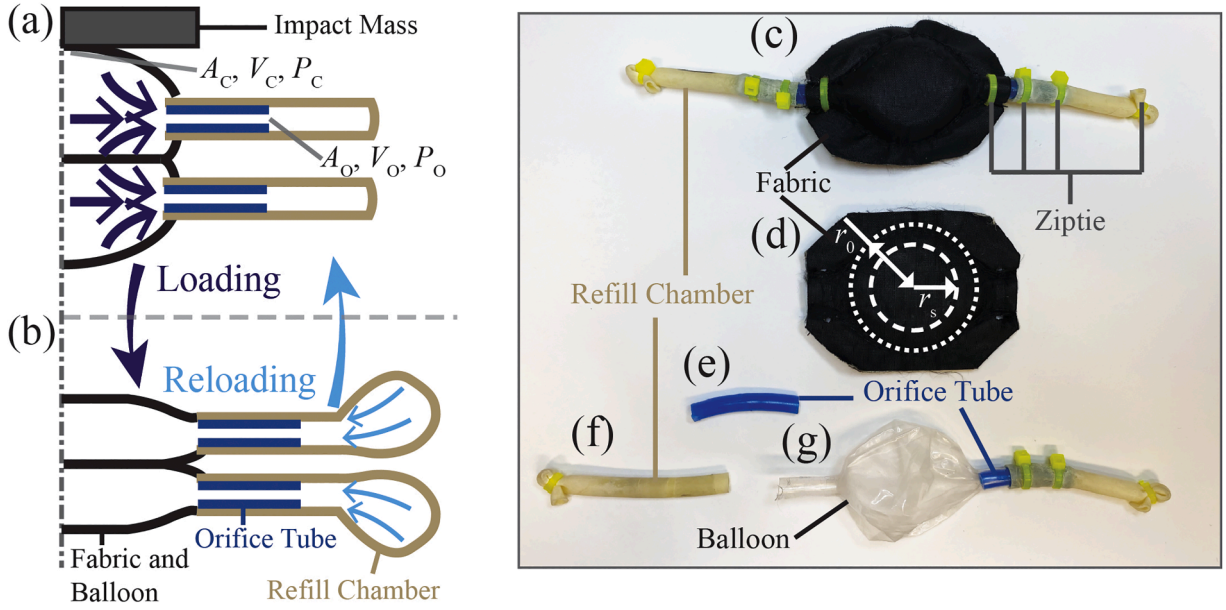

Fig. 1. Schematic of the Soft Hydraulic Shock in loading (a) and reloading (b). A_O, V_O, and P_O represent area, velocity, and pressure at the orifice outlet, respectively; A_C, V_C, and P_C represent area, velocity, and pressure at the contact area, respectively. The arrows in the fabric and balloon in (a) indicate the fluid flow through the orifice, and the arrows in the refill chambers in (b) indicate the flow going back to the balloon after the impact. Detailed assembly of the prototyped device is shown in (c–g). Details of the materials used in (c–g) can be found in Section 2.1.

impact masses of 2.59 and 3.65 kg. Two repeat impacts were performed at each velocity-mass impact condition. Specific details of the drop tower test apparatus, data processing methods, and justification of impact loading conditions can be found in the Supplementary Materials Section S2, including Fig. S1.

To compare the Soft Hydraulic Shock with other state-of-the-art shock absorbing technologies currently used in helmets, we tested five shock absorbers found in commercially available football helmets using the same test protocol. One of the shock absorbers, the 3D Printed Lattice, was larger than the impact mass in its original form, so it was cut to a smaller size to ensure that it fit within our test setup and was of a similar size to the other tested shock absorbers. The other four shock absorbers were manufactured as discrete shock absorber units and removed from their respective helmets for testing. The height, mass, and cross-sectional area for each tested shock absorber were measured prior to testing; details of all tested shock absorbers are provided in the Supplementary Materials Section S3, including Table S1. Because the other shock absorbers were extracted from their respective helmets, rather than being designed specifically for this study, we could not control their original dimensions.

For each impact test, the energy absorption ratio, which describes how much a shock absorber dissipates impact energy and suppresses rebounding of the impact mass, was calculated by

$$Energy\ Absorption\ Ratio = \frac{E_{\text{Absorbed}}}{E_0} \times 100\% = \left(1 - \frac{E_{\text{Rebound}}}{E_0}\right) \times 100\%, \tag{2}$$

where E_0 is the initial kinetic energy when the impact mass reaches the top of the shock absorber. Measured initial impact speeds obtained from high-speed video recordings were used to calculate E_0. E_{Rebound} is the remaining kinetic energy when the impact mass reaches the original shock absorber height in rebounding. In cases where the impact mass did not surpass the original shock absorber height, E_{Rebound} was set to zero. E_{Absorbed} is the difference between E_0 and E_{Rebound}.

Most helmets are intended to protect the human head not only at ambient temperature, but also at sufficiently high and low temperatures representative of changes in weather and geographical location. Therefore, in addition to ambient temperature testing at a room temperature of 19.5 °C, all six shock absorbers were tested after extended exposure to -18 °C and 50 °C environments, considering the temperature range in which human recreational activities usually occur. All shock absorbers were kept in a freezer set to -18 °C (for the cold temperature condition) and an incubator set to 50 °C (for the hot temperature condition) for over 24 h to ensure the shock absorbers reached the aimed temperature. Then, the shock absorbers were tested twice at each of the six impact conditions (i.e., mass-velocity combinations) within 60 s of removal from the freezer or the incubator. The variations of energy absorption ratio at -18 °C and 50 °C from the ambient temperature were calculated to describe the consistency of shock absorber performance in hot and cold environments.

2.3. Parametric analyses based on FE modeling

To explore the effects of changing orifice area, fabric longitudinal modulus, impact mass, and impact velocity on the resulting force, maximum compression, and pressure within the Soft Hydraulic Shock, we developed and validated a FE model of the Soft Hydraulic Shock (Fig. S2) and performed groups of simulation impact tests. In the FE model, discharge coefficient, C_d, and fabric longitudinal modulus of the FE model were determined by fitting the model to the results of the experimental tests. Further specific details regarding the design of the FE model, such as model geometry and material properties, can be found in the Supplementary Materials Section S4, including Fig. S2 and Table S2. Because the Soft Hydraulic Shock exhibited a 100 % energy absorption ratio across all loading conditions experimentally, we investigated the effect of the various parameters on the peak force of the impact response.

2.3.1. Influence of orifice area

Orifice area is a key parameter in determining the resulting impact force of the Soft Hydraulic Shock. As the orifice area increases, the pressure and the force contributed by the orifice decrease according to Eq. (1). As a result, the Soft Hydraulic Shock will be compressed a greater amount. Considering the buckling of the fabric during compression, we expected to see that the self-contact of the fabric would dominate the contact force peak when the Soft Hydraulic Shock was compressed to a specific location, and we define this phenomenon as “bottoming-out”. Once bottoming-out occurs, the impact energy is no longer dissipated by the orifice and the contact force increases. Therefore, it is critical to find how the orifice area affects the critical compression location. We performed simulations with a wide range of orifice areas at the impact speed of 1.9 m/s and impact mass of 2.59 kg to investigate how orifice area affects the peak force, the maximum compression location, the pressure, and the profiles of the force-displacement and pressure-displacement curves.

2.3.2. Influence of fabric longitudinal modulus

The high pressure inside the Soft Hydraulic Shock stretches the fabric during an impact, and this stretching affects the volume flow rate, which in turn affects the force according to Eq. (1). Therefore, we varied the fabric longitudinal modulus in simulations under the impact speed of 1.9 m/s and the impact mass of 2.59 kg to investigate how the stretch of the fabric influences the response of the Soft Hydraulic Shock. We found that the fabric transverse and shear moduli do not influence the magnitude of the peak force, the location of the peak force, and the maximum compression location. Therefore, the longitudinal modulus was used to represent the stretchability of the fabric.

2.3.3. Influence of loading parameters

In the drop tests, the impact loading is quantified by two variables: impact mass and impact speed. To show how the peak force scales according to impact mass and impact speed, we ran FE simulations with impact masses of 1–5 kg, and impact speeds of 1–5 m/s. The peak force for each loading was calculated and regressions were performed to determine how peak force is influenced by impact speed and impact mass independently.

To further explore how impact mass and impact speed affect the force-displacement curve, two groups of simulations were performed with controlled impact energies, but different combinations of impact mass and impact speed. In one group, the impact mass was kept constant (2.5 kg) while the impact velocity increased (2.0, 2.8, 3.5, 4.0 m/s), which resulted in impact energies of 5, 10, 15, and 20 J, respectively. In the other group, the impact velocity was kept constant (2.0 m/s) while the impact mass increased (2.5, 5.0, 7.5, 10.0 kg) to achieve the same variation in impact energies (5, 10, 15, and 20 J, respectively).

2.3.4. Optimization of the Soft Hydraulic Shock

The orifice area in Eq. (1) is one of the most important parameters of the Soft Hydraulic Shock. It can be easily adjusted by using different sizes of orifice tubes. Therefore, we conducted an optimization task to minimize the peak force by tuning the orifice size. The optimizations were performed at impact masses of 1, 2, 3, 4, and 5 kg and impact speeds of 1, 2, 3, 4, and 5 m/s. A wide range of orifice areas (2 mm^2 to 150 mm^2 in increments of 2 mm^2) was searched, and the minimum peak forces were compared with the original peak force from impacts to the Soft Hydraulic Shock with an orifice size equal to that of the physical prototypes.

2.4. Translation to head impact protection

To explore how the Soft Hydraulic Shock performs in a wearable PPE

application, we used laboratory test headforms and a pneumatic linear impactor to conduct impact tests representative of American football impacts. Using head kinematics from the test headforms to compute various brain injury risk metrics, we characterized the impact performance of a single Soft Hydraulic Shock alongside the five state-of-the-art shock absorbers also tested in drop tests (Fig. 10a). We then prototyped two methods of integrating the Soft Hydraulic Shock into an American football helmet: a replacement for energy-absorbing comfort pads (Fig. 11b) and a modified chinstrap (Fig. 12a, b). Comfort pads from a youth American football helmet were replaced with Soft Hydraulic Shocks of similar height and cross-sectional area and tested at the full helmet level; additional tests were conducted at the unit level to determine how much energy absorption ratio could be improved by replacing comfort pads with the Soft Hydraulic Shock. The helmet models used for materials in unit level tests are listed in Table S3. To prototype a chinstrap, existing foam from inside a chinstrap was removed and replaced with a single Soft Hydraulic Shock, then affixed to a youth American football helmet. Both prototype embodiments had their impact performance individually tested and compared against unmodified helmets. The head kinematics from each impact test were collected and used to compute various brain injury risk metrics, including Head Acceleration Response Metric (HARM) [32], Diffuse Axonal Multi-Axis General Evaluation (DAMAGE) [51], Head Injury Criterion (HIC) [52], and peak angular acceleration (PAA). The details of the test setup and the prototype development are provided in the Supplementary Materials Section S7.

3. Results

Using a drop tower test methodology, prototypes of the Soft Hydraulic Shock and five other state-of-the-art shock absorbers were individually tested at six different impact loadings and three different temperature conditions. Calculated energy absorption ratios from each impact test are reported, along with analyses of force-displacement curves.

FE modeling was used to develop a validated model of the Soft Hydraulic Shock. Simulation impact tests were used to explore the effect of various design parameters and impact loadings on the impact response of the Soft Hydraulic Shock. FE modeling was also used to perform an optimization of the orifice area for reducing peak impact force under different impact loadings. The validation results, effects of changing design parameters, and optimized orifice areas are reported.

The Soft Hydraulic Shock was then tested for its ability to mitigate brain injury risk. The Soft Hydraulic Shock and each of the five other shock absorbers tested in drop testing were individually affixed to a test headform and impacted with a pneumatic linear impactor. The Soft Hydraulic Shock was also implemented into a youth American football helmet as a replacement for existing energy-absorbing comfort pads and an improved chinstrap. Reductions in kinematics-based brain injury risk metrics are reported.

3.1. Impact responses at different impact speeds and masses

Energy absorption ratios for each shock absorber and impact condition are compared in Fig. 2. The Soft Hydraulic Shock exhibited 100.0 % energy absorption at all loading conditions. The average energy absorption ratio for the other shock absorbers across all loading conditions (masses, speeds, and temperatures) were 75.3 % (3D Printed Lattice), 88.7 % (Rheon Shock), 74.0 % (Single Stage Shock), 75.8 % (Dual Stage Shock) and 90.0 % (XRD Pad). Since the impact velocity was controlled by the drop height of the mass, the mean absolute error of the actual velocity relative to the aimed velocity was 2.1 %. Aside from the Soft Hydraulic Shock, the energy absorption ratio varied with impact speed (1.3 %–2.5 %) and mass (2.6 %–10.1 %). The energy absorption ratio

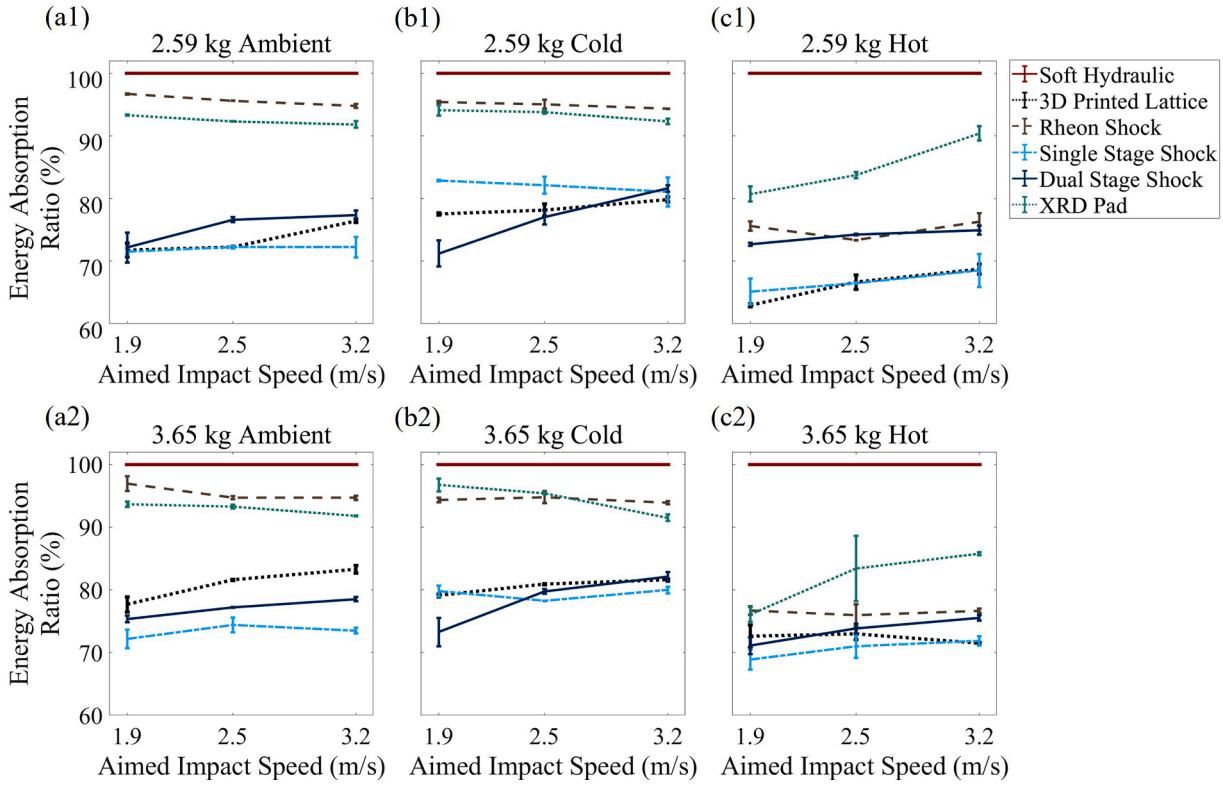

Fig. 2. Energy absorption ratio of the Soft Hydraulic Shock and five state-of-the-art shock absorbers at different temperature conditions (a = ambient [19.5 °C], b = cold [-18 °C], c = hot [50 °C]), impact masses (2.59 kg: a1, b1, c1; 3.65 kg: a2, b2, c2), and impact speeds (1.9, 2.5, 3.2 m/s). Error bars indicate the standard deviation across two repeat impacts per loading condition. The energy absorption ratio of the five other shock absorbers varied according to the impact speed, mass, and temperature condition. The Soft Hydraulic Shock maintained a 100 % energy absorption ratio across all tested conditions.

increased with speed in most cases, except the XRD Pad and the Rheon Shock in ambient and cold conditions and the Single Stage Shock at the 2.59 kg cold impact condition.

To further examine the difference in impact responses, the force-displacement curves for all six shock absorbing technologies at the ambient temperature, 2.59 kg mass, and 1.9 m/s speed impact condition are plotted in Fig. 3, with photos of each shock absorber corresponding to the times of the beginning of the impact, the peak force, and the maximum compression. The displacement coordinate system was established with the positive direction vertically downwards (i.e., pointing towards the base of the testing apparatus). The origin coordinate (displacement = 0) was set as the base of the force plate and therefore all displacements were negative. For all shock absorbers, the force increased gradually with increasing displacement at the beginning of the impact process. After the peak force, the force decreased with increasing displacement in the Soft Hydraulic Shock, while the force decreased with decreasing displacement (3D Printed Lattice, Single Stage, Dual Stage) or relatively constant displacement (Rheon and XRD) in the other shock absorbers. Furthermore, it should be noted that the maximum compression location occurred when the force was almost zero in the Soft Hydraulic Shock. Meanwhile, the maximum compression location occurred at a force approximately the same as the peak force in the 3D Printed Lattice, Single Stage Shock, and Dual Stage Shock, and at a force between approximately one-half and two-thirds of the peak force in both the Rheon and XRD shocks.

Additionally, in order to verify the applicability of Bernoulli's equation to the flow in the Soft Hydraulic Shock, we utilized the average flow velocity to calculate the Reynolds number. The average flow velocity was estimated by assuming that all the fluid was expelled from the central balloon at the time of maximum compression. Then, the dynamic

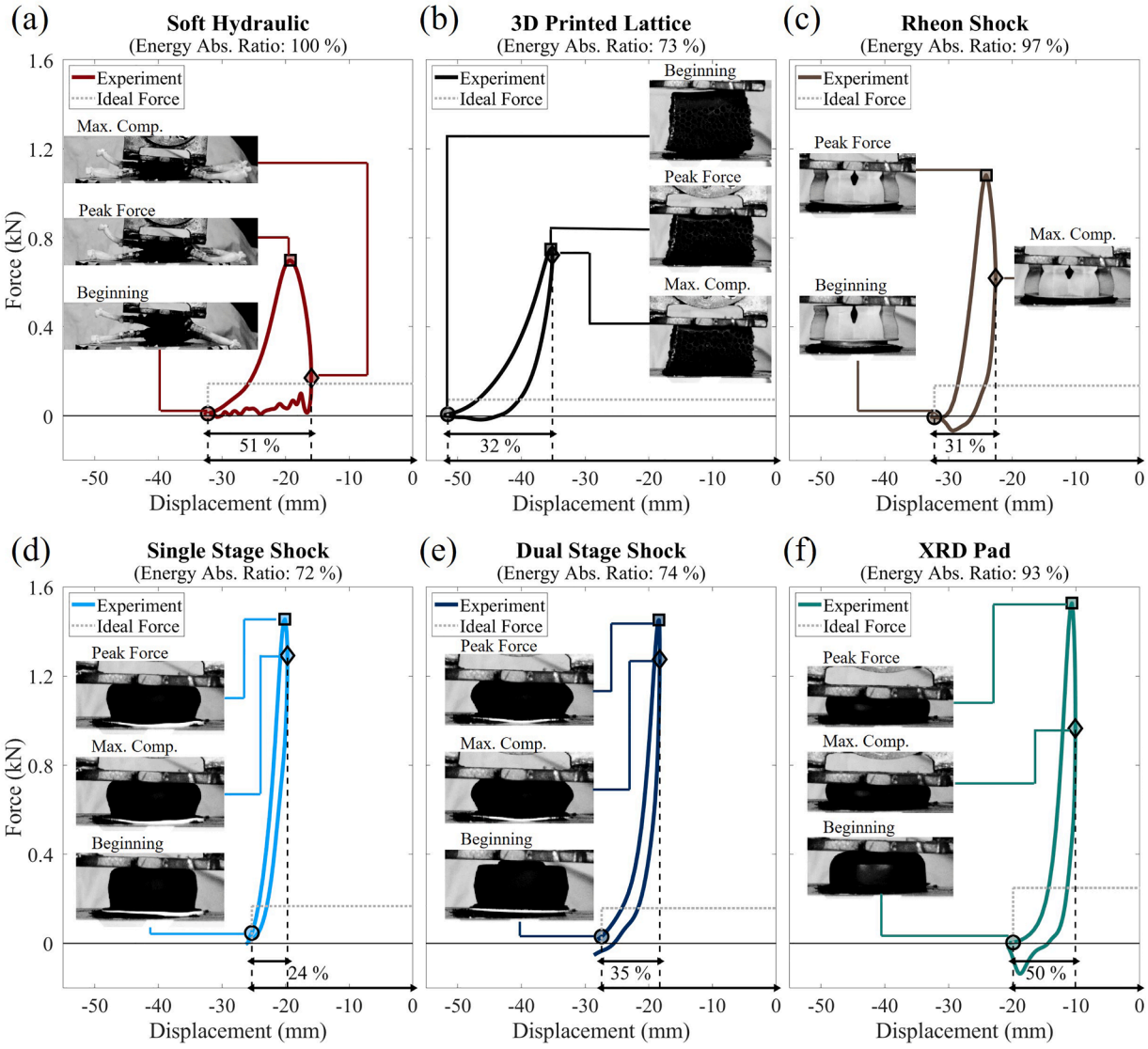

Fig. 3. The force-displacement curves of each shock absorber at a loading condition of 2.59 kg and 1.9 m/s at ambient temperature. Pictures of the shock absorbers at the Beginning (denoted by a circle), the Peak Force (denoted by a square), and the Maximum Compression locations (Max. Comp., denoted by a diamond) are shown in their respective plots. The energy absorption ratio (Energy Abs. Ratio) in the corresponding impact is recorded below the title. The maximum compression ratio, which is the utilized stroke divided by the initial height of the shock absorber, is shown on the bottom of each plot, above the x-axis. The vertical black dashed lines in each plot indicate the initial height and the maximum compression location of the shock absorber in the impact. The dotted rectangle in each plot indicates the ideal force-displacement curve for the given shock absorber height. In (a), the Soft Hydraulic Shock continues to absorb energy after the Peak Force location (displacement continues to increase), and no rebound is observed (the force is close to zero at the Maximum Compression location, where the velocity is zero). In the other shock absorbers (b-f), little energy absorption can be observed after the Peak Force location, and there is substantial rebounding (the force is still high at the Maximum Compression location, which will cause the impact mass to rebound).

viscosity of 0.056 kg/(m·s) for propylene glycol and the characteristic linear dimension of 4 mm (the diameter of the orifice) were used to calculate the Reynolds number. The average Reynolds number over all tests was 3576.09 (>>1) (Supplementary Materials Section S8, Table S4). This suggests that the flow is dominated by inertial forces, so the pressure-volume rate relationship derived from Bernoulli's equation applies.

3.2. Variations of impact responses across temperatures

The variations in energy absorption ratio among the six different shock absorbing technologies between ambient (19.5 °C) and hot (50 °C) / cold (-18 °C) temperature conditions are shown in Fig. 4. The Soft Hydraulic Shock was found to yield a consistent performance in both hot and cold temperature conditions, exhibiting an energy absorption ratio of 100 % in all tests. For most of the other shock absorbers, the energy absorption ratios were improved at the cold temperature condition and deteriorated at the hot temperature condition. Force-displacement curves are plotted for each shock absorber at each temperature condition at the 2.59 kg, 1.9 m/s loading condition in Fig. 5. The shapes of the Soft Hydraulic Shock's force-displacement curves were nearly identical for the hot and ambient temperature conditions; a small increase in force and decrease in maximum displacement could be seen at the cold temperature condition. For all commercially available shock absorbers, greater compression could be observed at the hot temperature condition, and obvious hardening effects were found at the cold temperature condition, leading to increased force and reduced maximum displacement. The Dual Stage Shock had minimal changes in peak force across all three temperature conditions, but this was not observed in impact tests at higher speeds.

3.3. Development and validation of FE model

A FE model of the Soft Hydraulic Shock was developed for the ambient temperature condition from the physical experiments, as shown in Fig. 6. This model was used to measure the fluid pressure of the Soft Hydraulic Shock during impact and investigate the influence of orifice size and impact loading on shock absorber performance. Because the Soft Hydraulic Shock exhibited a 100 % energy absorption ratio across all impact conditions in the experimental tests, the focus of the FE model testing was on investigating and improving the force attenuation capabilities of the device. The orifice discharge coefficient (C_d) and the fabric longitudinal modulus (E_f) were determined by matching the FE results with the drop tower test results. As mentioned above, the Soft Hydraulic Shock was impacted at three impact speeds and two impact masses. We calculated the relative errors of peak force and maximum compression location for each repeat trial of each impact condition and averaged them across all the tests. A C_d value of 0.43 and an E_f value of 2.4 GPa were adopted because they minimized the sum of 50 % of the relative error of the peak force, 25 % of the relative error of the displacement where the peak force occurs, and 25 % of the relative error of the value of the maximum compression location, as shown in Fig. S3. Other combinations of weights were tested in Figs. S4–S7. Assigning equal weight to each of the three errors yielded identical values for C_d and E_f. However, assigning 100 % weight to any single error while neglecting the other two led to distinct C_d and E_f values, producing more

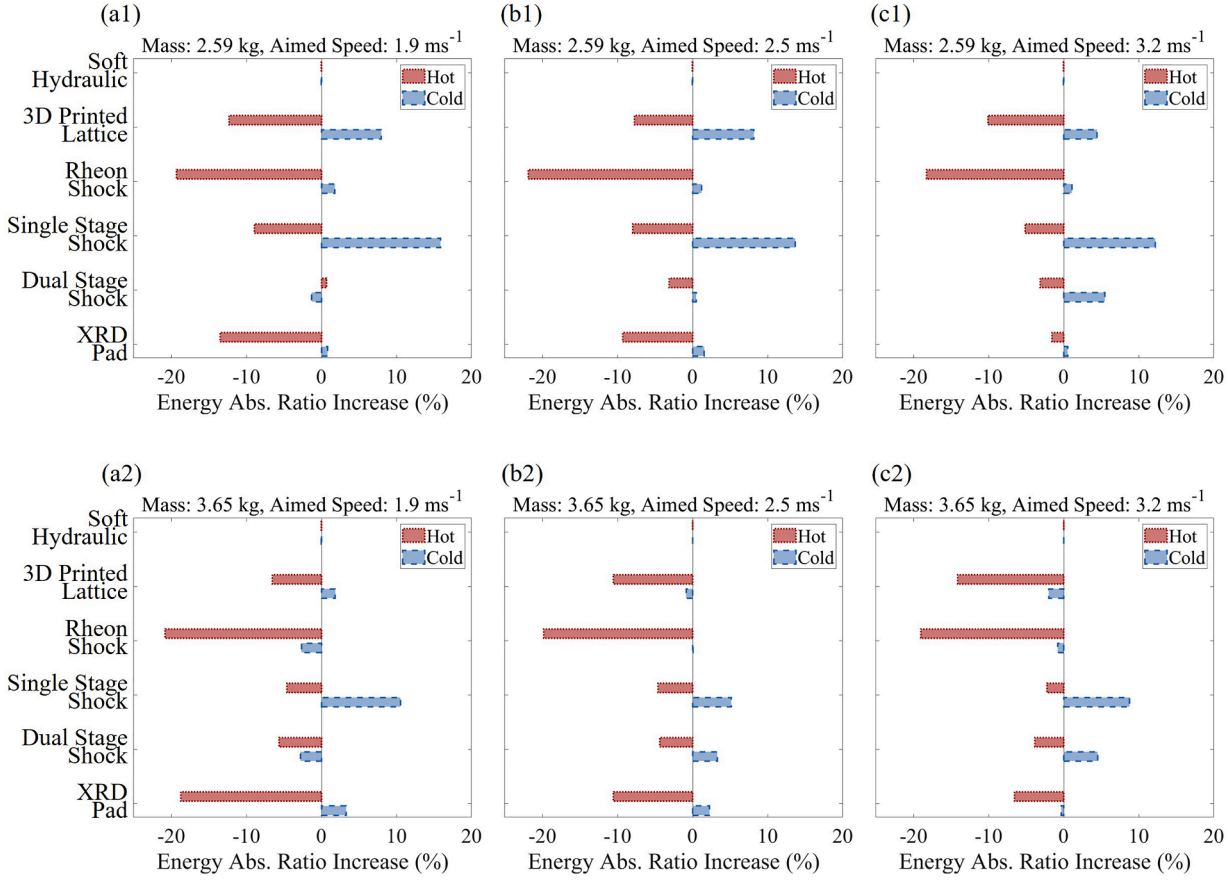

Fig. 4. Mean variation of energy absorption ratio for different shock absorbing technologies after 24 h exposure to cold (-18 °C) and hot (50 °C) temperature conditions at various impact loadings, relative to ambient (19.5 °C) temperature experiments. Experiments were conducted at six loading conditions for each temperature: two masses (1: 3.65 kg, 2: 2.59 kg) and three speeds (a: 1.9 m/s, b: 2.5 m/s, c: 3.2 m/s). The Soft Hydraulic Shock has a stable performance across the varying temperature conditions, while the other shock absorbers vary as much as 20 % in energy absorption ratio with changing temperatures.

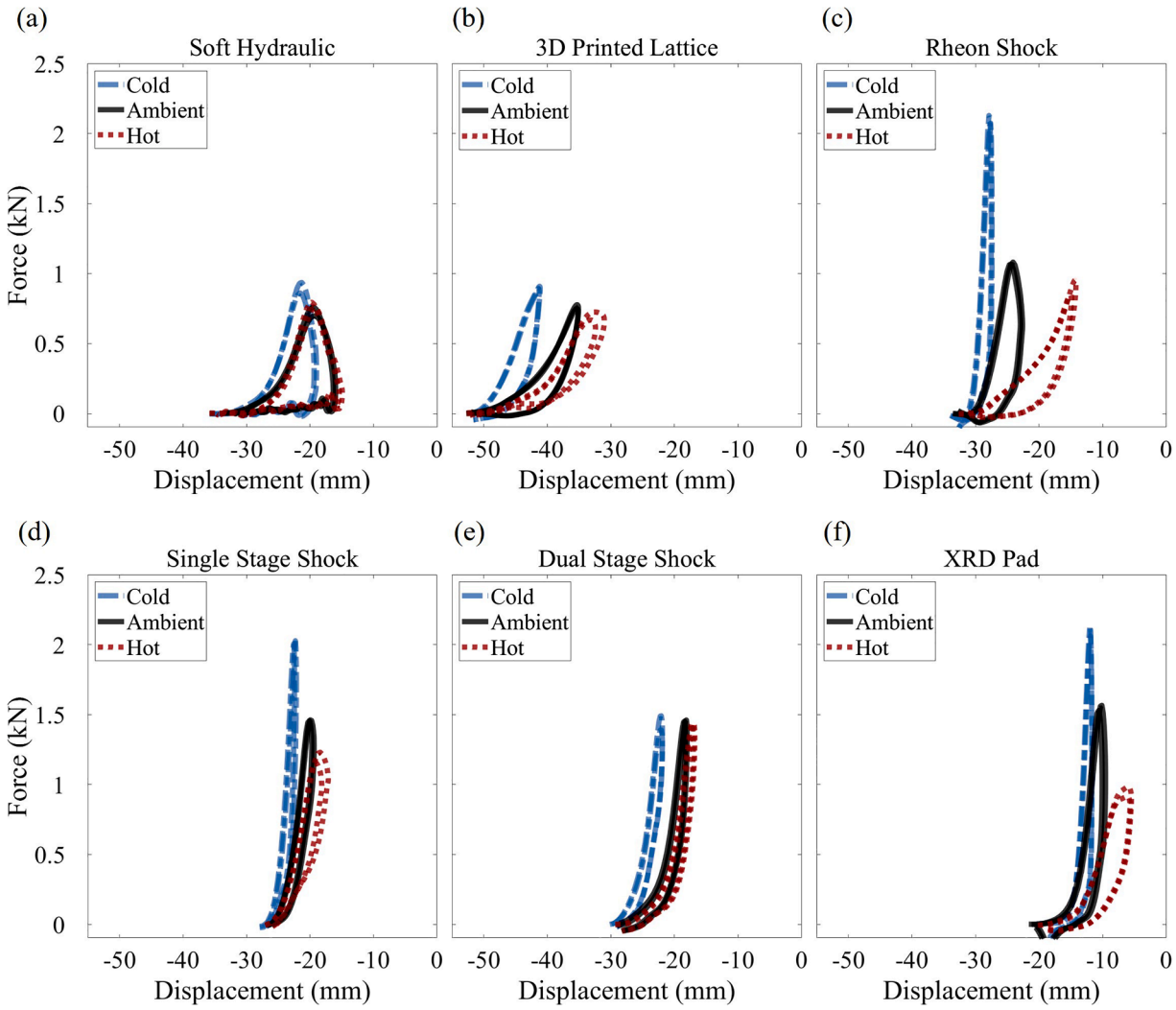

Fig. 5. Force displacement curves for an impact loading of 2.59 kg and 1.9 m/s at cold (-18 °C, blue dash-dot lines), ambient (19.5 °C, black solid lines), and hot (50 °C, red dotted lines) temperature conditions for the six different shock absorbing technologies. The curves for the two repeat trials in each of the cold, ambient, and hot temperature conditions are plotted; therefore, overlapping of the same type of curves can be seen. The force-displacement curve of the Soft Hydraulic Shock remained relatively constant at the hot and ambient temperature conditions, with small changes at the cold temperature condition.

pronounced disparities in the force-displacement curves from the physical experiments. The C_d and E_f values obtained were within the ranges of other materials and designs reported in previous studies [53–55]. We have also confirmed that other parameters, including the transverse modulus, shear modulus, and frictional coefficients, have little effect on the impact response of the Soft Hydraulic Shock (Fig. S8). To validate the impact response of the FE model, the force-displacement curves were plotted for each impact loading in Fig. 6. It is clear that the FE model could closely follow the rising and falling edges of the curves and could accurately predict the peak force and the maximum compression location for different impact masses and velocities. The energy absorption ratio was confirmed to be 100 % in every simulation, similar to the experimental results. Under the impact loading of 2.59 kg and 1.9 m/s (Fig. 6a1), the equivalent strain at the times of the beginning, the peak force, and the maximum compression were plotted and buckling of the fabric could be observed.

3.4. *Influence of orifice area, fabric modulus, and impact loading*

The orifice area and fabric longitudinal modulus were varied at a constant impact loading (2.59 kg, 1.9 m/s) to see how they influenced the impact response of the Soft Hydraulic Shock (Fig. 7). Increasing the orifice area led to an increase in maximum compression location and a decrease in peak force until a critical orifice area was reached (at which point the minimum peak force was achieved) (Fig. 7a1). Different from the peak force, the peak pressures in the top and bottom stack of the Soft Hydraulic Shock were similar to one another and monotonically decreased with a larger orifice area (Fig. 7a2). To further investigate the different variations of peak force and peak pressure with the orifice area, the force-displacement (Fig. 7c1) and pressure-displacement of the top (Fig. 7c2) and bottom (Fig. 7c3) stacks were plotted for three representative cases. The rapid increase of peak force that is observed when the orifice area is large is due to the occurrence of bottoming out at the end of the shock absorber's deformation.

When the fabric longitudinal modulus is varied, the peak force, maximum compression location (Fig. 7b1), and peak pressure (Fig. 7b2) change a small amount. Softening the fabric affected the force-displacement curve (Fig. 7d1) and the pressure-displacement in the top (Fig. 7d2) and bottom (Fig. 7d3) stacks by delaying their peaks, which can be attributed to the soft fabric allowing expansion of the shock so more fluid could remain in the shock instead of flowing through the orifice.

The influence of impact mass and speed on the force-displacement curves is shown in Fig. 8. While keeping impact velocity constant,

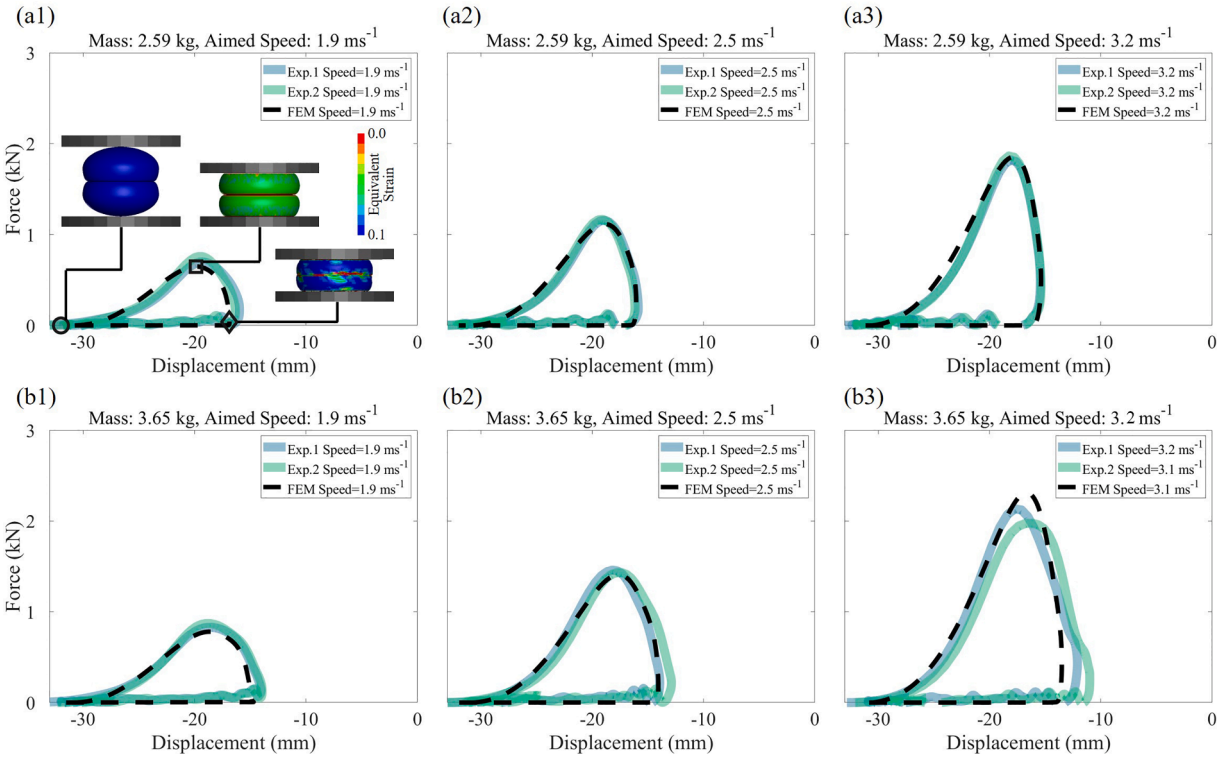

Fig. 6. Force-displacement curves of the Soft Hydraulic Shock under six loading conditions (a: mass = 2.59 kg; b: mass = 3.65 kg; 1: speed = 1.9 m/s; 2: speed = 2.5 m/s; 3: speed = 3.2 m/s) in simulation and physical experiments (two repeat trials). For the impact velocity of 1.9 m/s and impact mass of 2.59 kg (a1), the equivalent strain of the Soft Hydraulic Shock in simulation at the beginning (marked by the circle in the curve), the peak force (marked by the square), and the maximum compression (marked by the diamond) are plotted alongside the curve. The impact speed of the FE simulation and the two physical experiment tests are listed in the figure legends.

increasing impact mass kept the slope of the rising edge of the force-displacement curve similar, but increased the length of the rising edge of the curve (Fig. 8a). Keeping impact mass constant, increasing impact velocity changed the slope of the rising and falling edges of the force-displacement curve but had a small effect on the maximum compression location (Fig. 8b). Comparing the curves representing the same kinetic energy in Fig. 8, it can be seen that the peak force is more sensitive to changes in impact velocity and the maximum compression location is more sensitive to changes in impact mass. The scaling effects of the impact conditions on the force-displacement curves were further investigated using the FE model, and we found that the peak force was in a linear relationship with the impact mass and a quadratic relationship with the impact speed (Supplementary Materials Section S5, Fig. S9)

As the impact response is heavily influenced by the orifice area, an optimization to minimize the peak force by varying the orifice area was performed. Since the energy absorption ratio was found to always be 100 % if the Soft Hydraulic Shock does not bottom out, optimizations were performed solely for peak force. Impact masses ranging from 1.0 kg to 5.0 kg and impact speeds ranging from 1.0 m/s to 5.0 m/s were adopted in the optimization. Peak forces for the original orifice area were used as a baseline (Supplementary Materials Section S6, Fig. S10b) and large force reductions were observed when optimizing the orifice area (Figs. 9b, S10a). The optimized orifice areas are given in Fig. 9a, where the optimized orifice area was found to be mainly decided by the impact mass and kept relatively constant across different impact speeds. This finding agrees with the fact that the maximum compression location is almost unchanged with the increasing impact speed.

3.5. Translation to head impact protection

A single unit of each shock absorber was affixed to a Hybrid III headform and impacted by a linear impactor at a speed of 2 m/s (example shown in Fig. 10a), which represents mild head impacts in American football. This lower speed was also used considering only one shock absorber unit received the impact loading and not a full helmet. The linear and angular accelerations of the headform were recorded and processed (Fig. 10f–k), and the head kinematics were used to calculate HARM (a metric used to assess football helmet safety performance [32]), DAMAGE (an indicator of the brain strain [51]), and HIC (an indicator of severe head injury risk [52]). PAA, HARM, DAMAGE, and HIC are given in Fig. 10b–e, where the Soft Hydraulic Shock demonstrated favorable performance compared with the other shock absorbers, especially in terms of HIC.

Single-stack Soft Hydraulic Shocks were used to replace XPF Auxetic Foam comfort pads that were removed from LIGHT LS1-CY helmets (Fig. 11b). Helmets equipped with Soft Hydraulic Shocks and unmodified LS1-CY helmets were fit to a small NOCSAE headform and impacted by a linear impactor at three velocities representative of youth American football head impacts (Fig. 11a). To test if the helmet would meet comfort requirements typical of football helmets, the pressure between the headform and the individual Soft Hydraulic Shocks placed throughout the helmet was measured. The average pressure was 28.4 kPa (range: 12.4–42.9 kPa), which is below the helmet comfort thresholds observed by Jadischke et al. [56].

Two-way ANOVAs revealed statistically significant main effects of impact velocity ($p < 0.0001$) and comfort pad type ($p < 0.0001$) on DAMAGE, HARM, PAA, and HIC. Across all impact velocities, average reductions afforded by the implementation of the Soft Hydraulic Shock as a comfort pad were 25.0 % for DAMAGE, 23.9 % for HARM, 32.8 % for PAA, and 23.4 % for HIC. There was a statistically significant interaction between impact velocity and comfort pad type for DAMAGE ($F(2,39) = 19.16$, $p < 0.0001$), HARM ($F(2,39) = 18.96$, $p < 0.0001$), and HIC ($F(2,39) = 8.05$, $p = 0.0012$), but not for PAA ($F(2,39) = 2.25$, $p = 0.119$). Significant results of multiple comparison tests for each

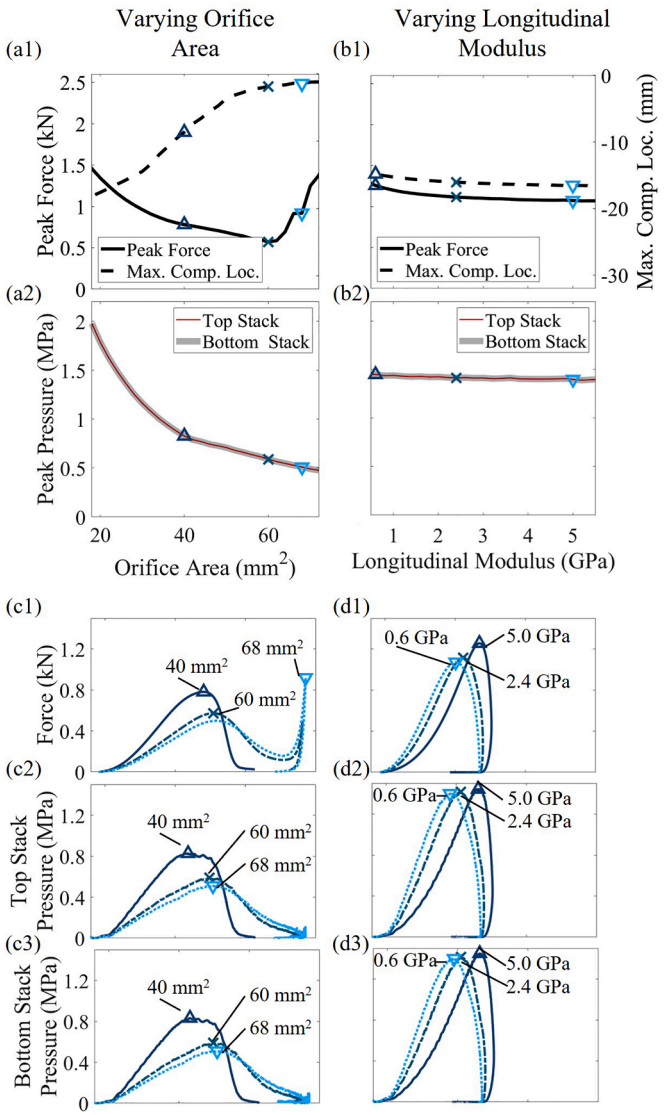

Fig. 7. Effect of changing orifice area and fabric longitudinal modulus on impact response of the Soft Hydraulic Shock. Variations of peak force (a1, b1, left axis), maximum compression location (a1, b1, right axis), and peak pressure (a2, b2) with changing orifice area and fabric longitudinal modulus under an impact velocity of 1.9 m/s and impact mass of 2.51 kg are shown. (c) shows example curves with different orifice areas, and (d) shows example curves for different longitudinal moduli of the fabric: the force-displacement curves (c1), and the pressure-displacement curves for the top stack (c2) and the bottom stack (c3) for the orifice areas of 40 mm^2, 60 mm^2, 68 mm^2 (longitudinal modulus: 2.4 GPa) are plotted; and the force-displacement curves (d1), and the pressure-displacement curves for the top stack (d2) and the bottom stack (d3) for the longitudinal moduli of 0.6 GPa, 2.4 GPa and 5.0 Gpa (orifice area: 12.57 mm^2) are plotted.

metric are displayed in Fig. 11c1–c4.

To further investigate the impact performance of the Soft Hydraulic Shock compared to existing comfort pads, unit-level tests were performed with the drop tower apparatus. The drop testing revealed that replacing the XPF Auxetic Foam with a Soft Hydraulic Shock increased the energy absorption ratio of the shock absorber–comfort pad system by an average of 13.5 % (Fig. 11d1). In three additional examples at the unit level, drop testing revealed that replacing energy-absorbing comfort pads from other helmets increased the energy absorption ratio of the shock absorber–comfort pad systems by an average of 8.5 % overall (Fig. 11d2–d4).

The chinstrap is an important energy-absorbing component for impacts to the front of a football helmet. Therefore, we prototyped chinstraps with a single-stack Soft Hydraulic Shock placed inside of them (Fig. 12b) for the purpose of attenuating impact severity during impacts in which the chinstrap takes considerable loading (e.g., impacts to the front of the facemask). Prototype and reference chinstraps were attached to a LIGHT LS1-CY helmet for testing (Fig. 12a). Inflation of the refill chambers could be observed for all facemask impacts, indicating compression of the Soft Hydraulic Shock during the impact process (Fig. 12c).

A two-way ANOVA revealed statistically significant main effects of chinstrap type ($p < 0.0001$) and impact velocity ($p < 0.0001$) on DAMAGE. At 1.6 m/s, the mean difference (95 % CI) in DAMAGE was 0.027 (0.013–0.041), corresponding to a mean DAMAGE reduction of 33.6 % by utilizing the Soft Hydraulic Shock chinstrap ($p = 0.0002$). At 5.0 m/s, the mean difference (95 % CI) in DAMAGE was 0.039 (0.025–0.053), corresponding to a mean DAMAGE reduction of 9.8 % by utilizing the Soft Hydraulic Shock chinstrap ($p < 0.0001$) (Fig. 12d). For DAMAGE, there was not a statistically significant interaction between the effects of impact velocity and chinstrap type ($F(1,36) = 1.94$, $p = 0.172$).

A two-way ANOVA revealed statistically significant main effects of chinstrap type ($p < 0.0001$) and impact velocity ($p < 0.0001$) on HARM. At 1.6 m/s, the mean difference (95 % CI) in HARM was 0.365 (0.107–0.623), corresponding to a mean HARM reduction of 28.1 % by utilizing the Soft Hydraulic Shock chinstrap ($p = 0.004$). At 5.0 m/s, the mean difference (95 % CI) in HARM was 0.663 (0.405–0.921), corresponding to a mean HARM reduction of 9.6 % by utilizing the Soft Hydraulic Shock chinstrap ($p < 0.0001$) (Fig. 12e). For HARM, there was not a statistically significant interaction between the effects of impact velocity and chinstrap type ($F(1,36) = 3.64$, $p = 0.065$).

4. Discussion

In this study, we applied the principle of pressure drop yielded by a fluid passing through an orifice to develop a novel, compact, and wearable hydraulic shock absorber that comprised soft components: the Soft Hydraulic Shock. In this section, we discuss the findings and implications of our extensive testing of this novel device. Under six different impact loadings (two masses, three velocities) and three different temperature conditions, the Soft Hydraulic Shock exhibited an energy absorption ratio of 100 %, a substantial improvement over five other state-of-the-art shock absorbers used in American football helmets. Furthermore, the energy absorption performance of the Soft Hydraulic Shock was consistent across cold, ambient, and hot temperature conditions. We developed a FE model of the Soft Hydraulic Shock and validated it according to the experimental results at various loading conditions, finding that the orifice area is the key parameter determining the shock absorber's performance. Across a range of impact loadings, the peak force was found to be in a quadratic relationship with the impact speed and in a linear relationship with the impact mass. Moreover, an optimization to minimize the peak force by varying the orifice area was performed for different combinations of impact masses and speeds, and we found that the optimized orifice does not change substantially with the impact speed. When the Soft Hydraulic Shock and the other state-of-the-art shock absorbers were attached directly to a test headform, the Soft Hydraulic Shock exhibited the lowest values for multiple injury risk metrics in impact tests, indicating its potential for use in head protective devices. Subsequently, the Soft Hydraulic Shock was integrated into a complete helmet system, serving as a replacement for comfort padding and an enhanced chinstrap. This integration notably reduced the severity of head impacts associated with low and high-velocity impacts common to youth American football.

The reaction force of the Soft Hydraulic Shock is determined by Eq. (1), which is formed based on three assumptions: (1) the flow follows Bernoulli's equation; (2) the square of the ratio between the orifice area and the contact area is negligible; (3) the difference between the actual

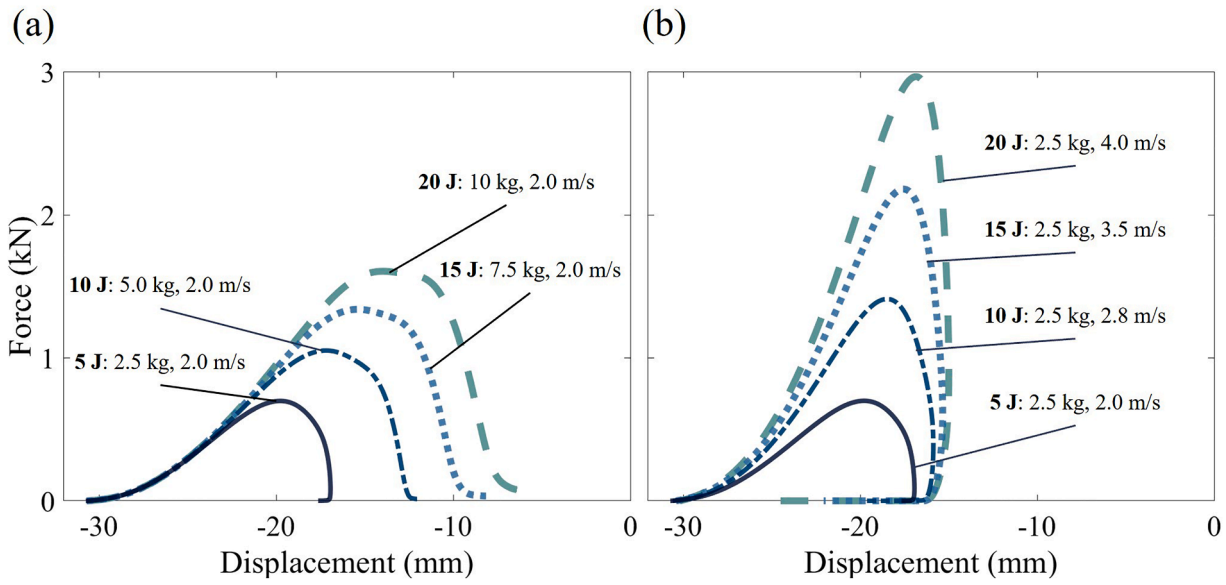

Fig. 8. Force-displacement curves of the Soft Hydraulic Shock in simulation experiments under increasing impact energies of 5, 10, 15, and 20 J with different combinations of impact velocities (2.0, 2.8, 3.5, 4.0 m/s) and masses (2.5, 5.0, 7.5, 10 kg) are shown. In (a), impact speed is kept constant and impact mass increases, which is shown to have a large effect on maximum compression. In (b), impact mass is kept constant and impact speed increases, which is shown to have a large effect on peak force.

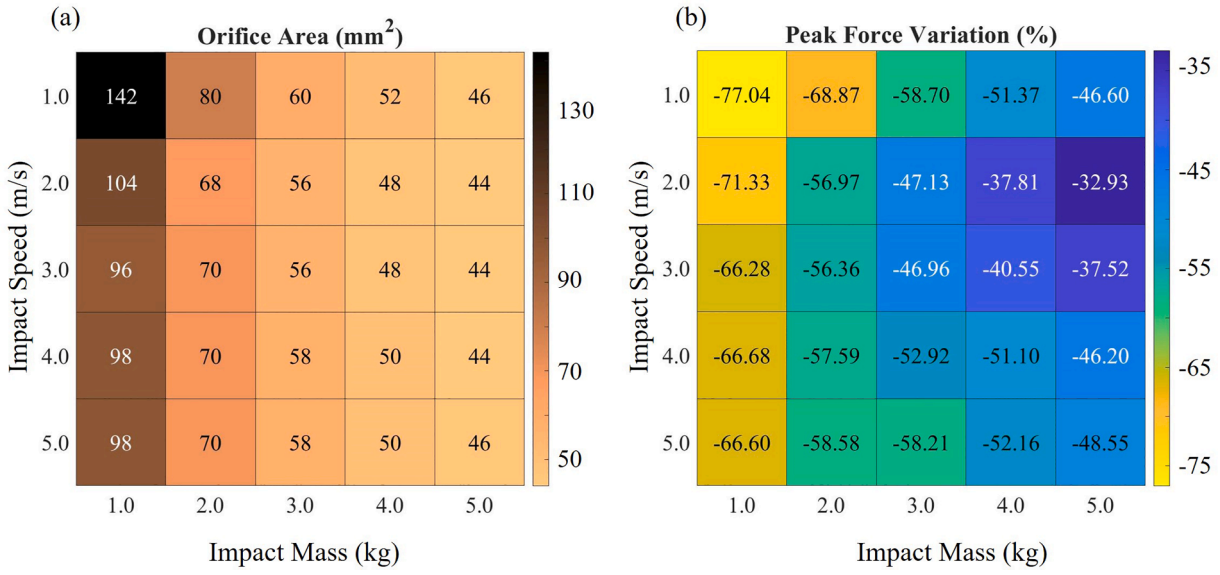

Fig. 9. Optimization to minimize peak force by varying the orifice size under different impact masses (1.0 to 5.0 kg) and impact speeds (1.0 to 5.0 m/s). The optimized orifice areas are in (a) and the percentages of peak force reduction afforded by the optimized orifice area, relative to the baseline area of 12.57 mm^2, are in (b). The optimized orifice area changes more with impact mass than it does with impact speed.

and the ideal discharge can be described with the discharge coefficient. The assumption that Bernoulli's equation applies to the Soft Hydraulic Shock is confirmed by estimating the Reynolds number to determine whether the flow is dominated by inertia or viscosity. As shown in Table S4, the average Reynolds number is 3576 and the smallest is over 2500. These numbers are much higher than a Reynolds number of 35, below which significant viscous effects have been observed [57]. Therefore, the flow is dominated by inertia and Bernoulli's equation applies to the impact response of the Soft Hydraulic Shock. It should be noted that the Reynolds number may get lower at the end of the shock absorber's compression because the impact mass has decelerated. However, the impact force is low at that time, and will not substantially affect the impact response overall. The assumption about the orifice area was made because a large contact area will occur at the very beginning of the impact. As shown in Fig. 1, the largest contact area is $\pi r_0^2 = 1521$ mm^2, and the actual contact area will quickly increase due to the internal pressure pushing and flattening the upper fabric to the impact mass. In contrast, the orifice area is approximately 13 mm^2. The assumption of the discharge coefficient was proposed in stationary flow and is widely used to simplify the analyses of pressure and velocity changes [53]. However, in our impact scenario, the flow varies significantly with time, so the discharge coefficient of the Soft Hydraulic Shock reflects an effect of the average discharge coefficient over the entire impact process. The validation of FE simulation supports this: a C_d of 0.43 can be used to accurately describe the force-displacement responses in six different impact loading conditions, which shows that the

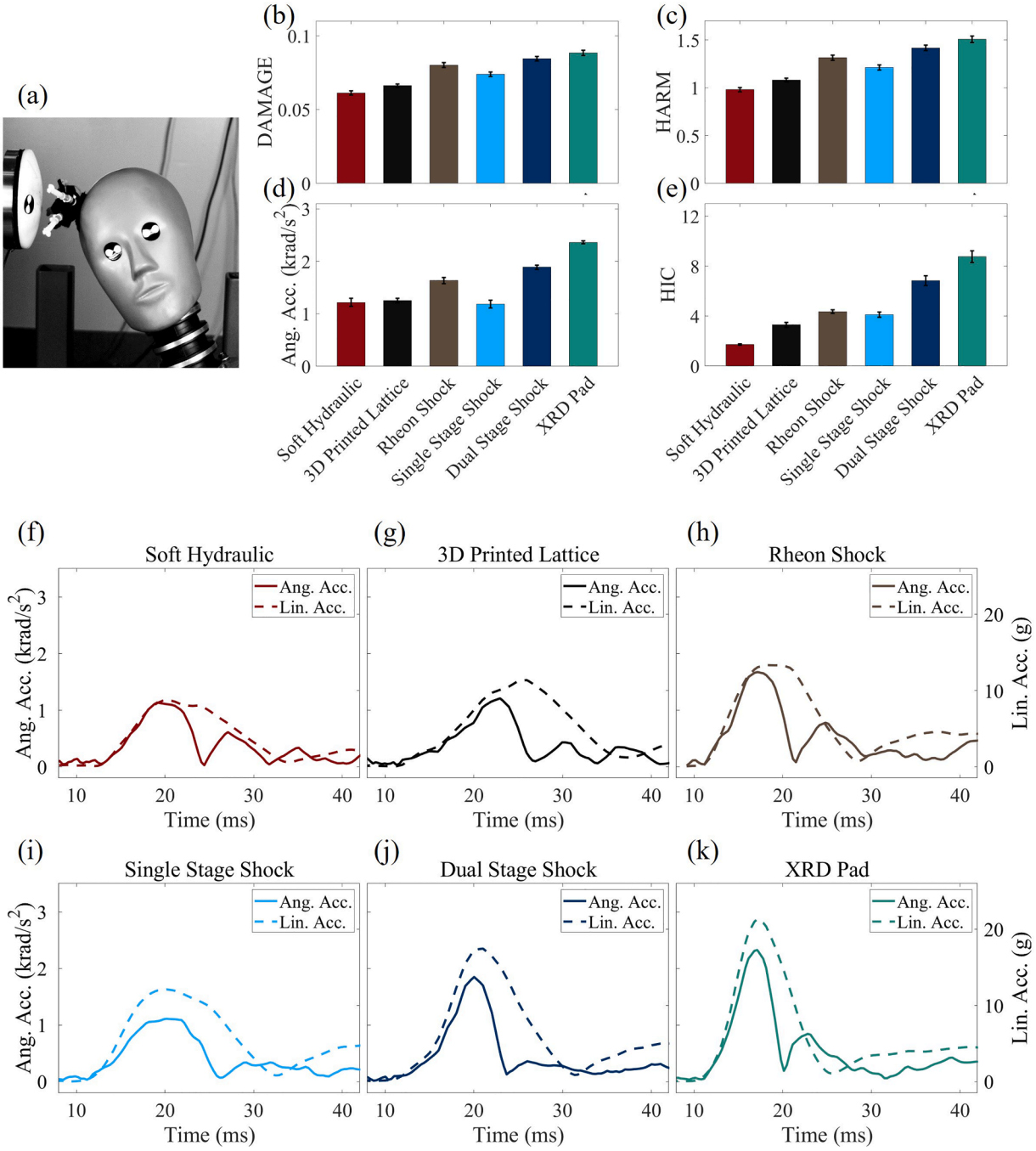

Fig. 10. Testing results from 2 m/s impacts to a Hybrid III headform protected by a single shock absorber. The impact experiment setup is shown in (a). DAMAGE (b), HARM (c), peak angular acceleration (d), and HIC (e) are shown for each of the six shock-absorbing technologies tested. (f–k) show examples of linear and angular headform accelerations plotted with time for each shock absorber tested.

assumption of discharge coefficient is applicable in this study. While Eq. (1) is succinct, directly solving it remains challenging as the contact area cannot be explicitly expressed. The determination of the contact area is influenced by the geometry of the shock absorber, the stretching of the fabric caused by the internal pressure, and the buckling of the fabric during compression. Consequently, we calculated the force-displacement responses using the FE model instead of analytical models.

Examining the force-displacement curve of a shock absorber is crucial because it demonstrates how an impact mass is decelerated and how it rebounds after impact. As shown in Fig. 3, the impact mass decelerates to static before maximum shock absorber compression and then accelerates upwards to rebound. As a result, the time point of the maximum compression divides the impact process into two phases: the compression phase and the rebound phase. The kinetic energy is stored or dissipated in the absorber during the compression phase, and any potential energy is transferred back to the impact mass during the rebound phase. The peak force always occurs during the compression phase, but, in the case of head protection, the force in the rebound phase may also contribute to injury risk [58], since the brain strain resulting from head impacts does not have a linear relationship with force and head kinematics [10].

In the compression phase, the area under the force-displacement curve (AUC) is the kinetic energy transferred from the impact mass to

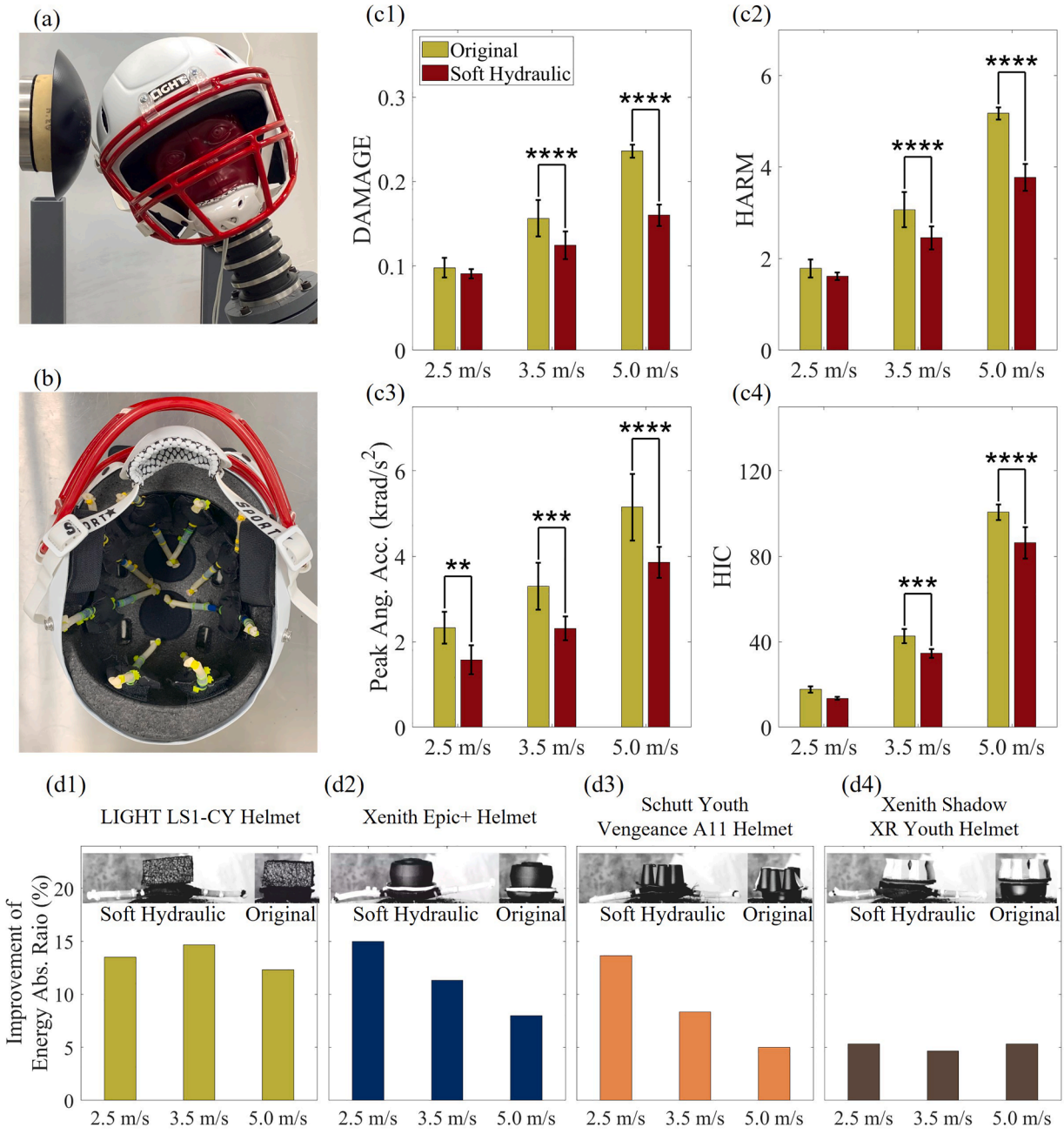

Fig. 11. Testing of the Soft Hydraulic Shock as a replacement for energy-absorbing helmet comfort pads. (a) Side upper impact location used for full helmet impact testing. (b) Interior view of a LIGHT LS1-CY youth football helmet with its comfort padding replaced by Soft Hydraulic Shocks. During impact tests, DAMAGE (c1), HARM (c2), peak angular acceleration (c3), and HIC (c4) were significantly lower in the LS1-CY helmet featuring Soft Hydraulic Shocks as comfort pads, relative to the original LS1-CY helmet (** $p < 0.01$, *** $p < 0.001$, **** $p < 0.0001$). (d1) In unit-level testing, the Soft Hydraulic Shock and the LS1-CY helmet's original comfort padding, XPF Auxetic Foam, were affixed to the helmet's shock-absorbing liner and impacted at the same velocities as full helmet testing. Replacement of the XPF Auxetic Foam with the Soft Hydraulic Shock was found to improve the energy absorption ratio. The energy absorption ratio was also improved in unit-level drop testing when the Soft Hydraulic Shock was compared to a thin Poron XRD comfort pad from a Xenith Epic+ helmet (d2), a SUREFIT + Poron comfort pad from a Schutt Youth Vengeance A11 helmet (d3), and a thicker Poron XRD comfort pad from a Xenith Shadow XR Youth helmet (d4).

the shock absorber. Because the kinetic energy is zero at the maximum compression location, where the speed of the impact mass is zero, the AUC between the beginning and the maximum compression is the impact energy. In this study, the shock absorbers that were tested demonstrated triangular-shaped curves, as depicted in Fig. 3. As the impact energies remained the same, the determination of the peak force was primarily dependent upon the compression ratio of the shock absorber. Accordingly, we observed that the Soft Hydraulic Shock and XRD Pad exhibited relatively high maximum compression ratios. To further minimize the peak force, it is imperative for the force to rise promptly so that the shape of the curve approximates that of a square, rather than a triangle. Additionally, the shock absorber should be compressed to a greater extent toward the end of the impact, as indicated by the dotted curves illustrated in Fig. 3.

In the rebound phase, because the kinetic energy of the impact mass is zero at the maximum compression location, the AUC of the force-displacement curve is the kinetic energy transferred back to the impact mass. According to Eq. (2), the energy absorption ratio is determined by the ratio between the AUCs of the compression and rebound phases. Fig. 3 shows that the rebound curve of the Soft

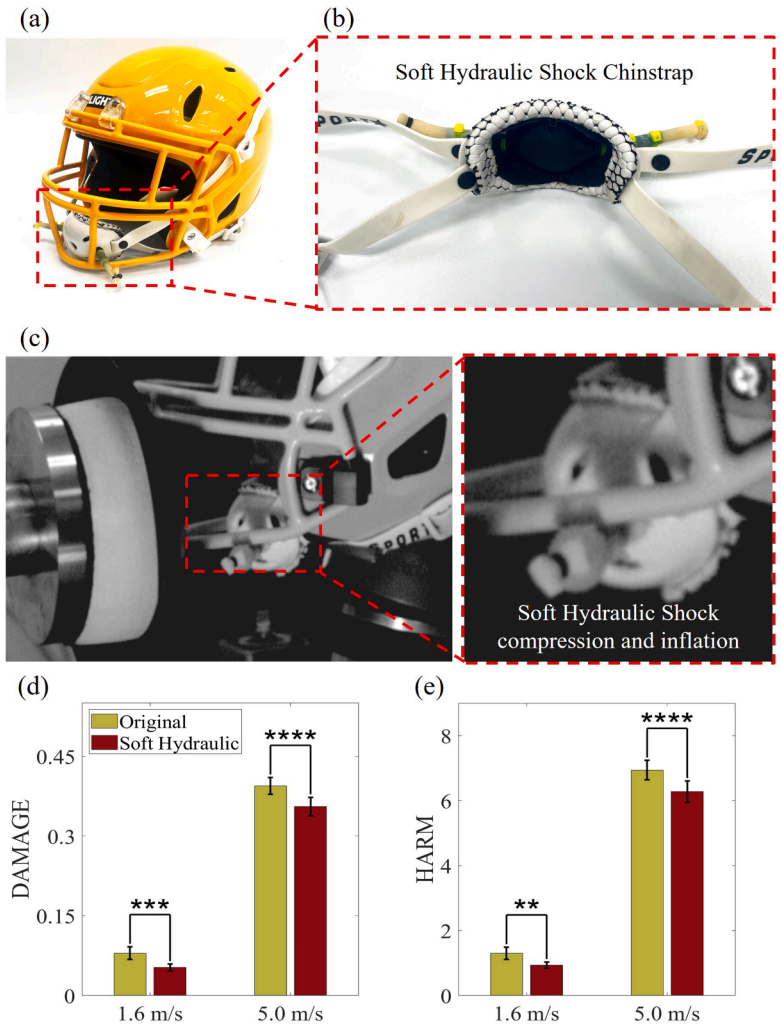

Fig. 12. Testing of the Soft Hydraulic Shock in a modified chinstrap. (a) Assembled LS1-CY youth football helmet with chinstrap featuring Soft Hydraulic Shock. (b) Interior view of chinstrap featuring Soft Hydraulic Shock. (c) Image taken from high-speed video footage showing compression of the central balloon and inflation of the refill chambers of the Soft Hydraulic Shock during an impact to the facemask of the helmet. DAMAGE (d) and HARM (e) were significantly attenuated during facemask impacts at both low and high impact velocities (** $p < 0.01$, *** $p < 0.001$, **** $p < 0.0001$).

Hydraulic Shock is close to a force of zero, which is distinctive from its compression curve. Therefore, the Soft Hydraulic Shock exhibited an energy absorption ratio of 100 %. For other shock absorbers, the compression curve closely resembles the rebound curve, particularly for the Single Stage Shock and the Dual Stage Shock. Consequently, their energy absorption ratios were lower. Furthermore, the force at the maximum compression location is crucial for the energy absorption of a shock absorber. Assuming that the force at the maximum compression location is zero, the velocity of the impact mass is zero as well, so the impact mass will remain static. On the contrary, a higher force at the maximum compression location will result in a significant rebound and lower energy absorption ratio. For the Soft Hydraulic Shock, according to Eq. (1), the force $F = 0$ when the contact velocity V_c=0, which suggests that no energy will be transferred back to the impact mass. In Fig. 3a, the force at the maximum compression location was close to zero but did not reach zero entirely because the buckled fabric makes contact with itself and there is potential contact with the orifice tube, cable ties, and refill chamber. A small fluctuation can be observed in the rebound phase because the refill chamber slowly pushes the liquid back into the balloon for the next impact. In the 3D Printed Lattice (Fig. 3b), Single Stage Shock (Fig. 3d), and Dual Stage Shock (Fig. 3e), the maximum compression occurred close to the peak force, which is similar to a fully elastic response. Accordingly, the impact mass was accelerated by a relatively high force during rebound, and the energy absorption ratio was lower. In the Rheon Shock (Fig. 3c) and XRD Pad (Fig. 3f), although the force at maximum compression was not as low as in the Soft Hydraulic Shock, it occurred at about 50 %–60 % of the peak force. Therefore, these two shock absorbers have relatively high energy absorption ratios. Small, negative force values at the end of the rebound phase could be observed in some shock absorbers when the displacement was close to the shock absorber height. This was likely due to the fact that the shock absorbers were attached to the force plate during the experiments, and the shock absorber itself may have moved upwards during rebound, pulling on the upper face of the force plate.

In certain applications, such as helmets, the performance of a shock absorber is expected by users to be consistent with varying temperatures. Considering this need, we tested the six shock absorbers across a temperature range with upper and lower limits representing extremes where human activities could occur (cold=-18 °C and hot=50 °C) and compared the energy absorption ratio with an ambient temperature condition (19.5 °C). In general, materials will soften at higher temperatures and stiffen at lower temperatures. Therefore, the energy absorption ratio will typically decrease with temperature for most shock absorbers. For shock absorbers that use structural deformation to absorb energy, the stiffening or softening of the materials will substantially influence the reaction force and maximum compression, which further

influences their energy absorption capabilities. Although previous research has been conducted to evaluate the performance of different helmet technologies across varying temperatures [59–61], we are not aware of any previously published studies detailing the temperature sensitivity of the 3D Printed Lattice, Rheon Shock, Single Stage Shock, or Dual Stage Shock. We observed relatively large variations in impact response for these shock absorbers when temperature was altered. XRD material is commonly used in a variety of sports helmets [62–64] and absorbs energy via a reversible phase change of urethane molecules, which is highly dependent on its glass transition temperature (near 0 °C). Under ambient temperature conditions, this material is highly effective, but upon exposure to low temperatures, XRD hardens and becomes less effective, as it has already transitioned into a glassy phase [59]. Therefore, XRD material has also been implemented in settings where temperature is largely controlled throughout use, such as in water polo [64], and varies in performance across high and low temperatures as shown in this study. In the Soft Hydraulic Shock, energy is dissipated by the fluid flowing through the orifice, which is only slightly affected by temperature as long as the fluid does not freeze. The freezing point of the propylene glycol used in the Soft Hydraulic Shock is below -18 °C; therefore, the Soft Hydraulic Shock performed consistently in both high and low temperatures as tested in this study. However, we observed small peak force variations, which could potentially have been caused by a change in the viscosity of the propylene glycol or hardening of the refill chambers, orifice tubes, or cable ties at the low temperature.

The Soft Hydraulic Shock was modeled and simulated by FEA to measure the fluid pressure in the device and further investigate the influence of the device parameters and impact loading on performance. Our analyses revealed that the orifice area and the longitudinal modulus of the fabric are the two most influential parameters on the impact behavior of the device (Figs. 7 and S8). We found that the size of the orifice area determines the shape of the force-displacement curve: when the orifice area was small (e.g., 40 mm^2), the pressure generated by the orifice dominated the reaction force, and therefore the force curve was similar to the pressure curve. With increasing orifice area (e.g., 60 mm^2), the peak force was reduced and a small corner of the force curve could be found at the maximum compression location with a non-zero force because of the self-contact between the fabric when it buckles. The force curve deviated from the pressure curve in this situation. When the orifice area got larger (e.g., 68 mm^2), this small corner would evolve into a tail in the force curve, and the peak of the tail would increase rapidly with the orifice area, which was defined as bottoming out. To reduce the peak force, the optimized orifice should be the one that makes the peak force generated by the orifice equal to that caused by the bottoming out. The longitudinal modulus of the fabric did not influence the Soft Hydraulic Shock's impact behavior as much as the orifice area, but a soft fabric will delay the peak force and pressure, because the liquid may remain in the Soft Hydraulic Shock by stretching the fabric and increasing the volume of the balloon, instead of flowing through the orifice. To efficiently use the stroke of the shock absorber, the force needs to rise faster, so a stiffer fabric is preferred.

The impact loading in the drop tests can be described by both the impact velocity and impact mass. The results from the simulation tests showed that the peak force had a linear relationship with the impact mass and a quadratic relationship with the impact speed (Fig. S9). This is similar to kinetic energy, which has a linear relationship with mass and a quadratic relationship with velocity. We believe this is beneficial for the protection of impacts at different speeds: the force of more severe, higher velocity impacts will be higher, but the Soft Hydraulic Shock will still be able to avoid bottoming out. To further analyze how impact mass and speed affect the Soft Hydraulic Shock's response, the kinetic energy was kept the same while the impact mass and speed were varied (Fig. 8). Increasing impact mass at a fixed impact speed appeared to proportionally affect the curve in both the force and displacement axes. Conversely, increasing impact speed at a fixed impact mass primarily influenced the curve in the force axis. Consequently, the peak force is more responsive to impact speed, while impact mass primarily dictates the maximum compression location, subsequently influencing the occurrence of bottoming out and the positioning of the force curve's corner.

The FE model of the Soft Hydraulic Shock was also optimized to reduce the peak force by varying the orifice area (Fig. 9) under different combinations of impact mass and speed, using the original orifice area (12.57 mm^2) as a baseline. We found that peak force reduction varied across impact loading conditions from -77 % to -32 % with a corresponding optimized orifice area, which indicates the potential to substantially improve the performance of the Soft Hydraulic Shock in the future. We also found that the optimized orifice area varies minimally with the impact speed, indicating that for a given orifice size, the Soft Hydraulic Shock is adaptive to varying impact speeds. This is because the impact mass determines whether the corner of the force curve occurs, as discussed above, which determines the optimized case. This speed-adaptive attribute is favorable for football helmet design because the impact mass is often the mass of another helmeted head, while the impact speed can range considerably.

Five technologies were tested in this study as references to the impact response of state-of-the-art shock absorbers used in helmets. Although energy absorption is commonly used to evaluate the performance of shock absorbers [44,65], it is difficult to translate this metric to a useful head or brain safety metric for several reasons, and the ability of our drop testing apparatus to represent realistic impact loading in a full helmet requires further investigation. In the drop tests, the impact mass impacted the shock absorbers in a single direction (i.e., vertically), only being accelerated by gravity. The shock absorbers were placed on a static and rigid force plate. In real head impacts, the loading on a helmet shock absorber is a result of contact with the helmet shell, which is constrained by a chinstrap and other connections. Friction between the interior surface of the shell and the shock absorber may cause a transverse force, which can result in shearing deformation of the shock absorber. The contact conditions between a helmet and an impacting surface are far more complicated than the conditions existing in our drop tower test apparatus [66]. Furthermore, the shock absorbers are worn on the head of the helmet wearer, which will translate and rotate quickly and has a moving center of rotation [13]. This is much different from the force plate, which remained static and affixed to the ground. Additionally, the impact loading in a full helmet is likely shared among several shock absorbers rather than being directed to a single unit. Because of this, we did not normalize the energy absorption ratio by the weight or cross-sectional area of the various shock absorbers. Finally, higher energy absorption ratios for the individual shock absorbers may imply milder impact severity for helmeted head impacts, but the relationship between energy absorption ratio and TBI risk is not entirely clear. In a head impact, the resulting head kinematics are influenced by both the neck and the force from the helmet, and an impact results in brain loading in a nonlinear relationship [10,67]. As an attempt to evaluate the protective ability of the shock absorbers investigated in this study, we simplified the problem by affixing a single unit of each shock absorber to a headform without any other helmet components (e.g., helmet shell, comfort padding, chinstrap, etc.). Since only one unit was included in this experiment while more shock absorbers are involved in a full helmet, we used a low speed (2 m/s), which is representative of mild head impacts in American football. The results shown in Fig. 10 suggest that the Soft Hydraulic Shock is effective in terms of DAMAGE, HARM, and angular acceleration, and efficiently minimizes the HIC metric. However, it should be noted that the relative efficacy in energy absorption ratio among the shock absorbers in the drop testing was not entirely the same in headform testing. For example, the Single Stage Shock had lower angular and linear accelerations than the Dual Stage Shock in headform tests; however, the two shared a similar energy absorption ratio. These results suggest that the relationship between the drop tower tests and the actual efficacy of a shock absorber in the context of head protection is complicated and warrants a more

comprehensive study.

The Soft Hydraulic Shock provided significant improvements in helmet safety when implemented into a full helmet system in two potential product applications. First, we removed the comfort padding from a helmet and replaced it with single-stack Soft Hydraulic Shocks. In many modern football helmets, including the LS1-CY helmet we used for full helmet testing, the comfort padding consists of highly engineered foams that are intended to both provide comfort to the user and dissipate impact energy. Our helmet testing results across a range of impact velocities demonstrated the ability of the Soft Hydraulic Shock to better attenuate injury risk metrics associated with both mild TBI and more severe TBI (i.e., skull fracture) when used in place of the LS1-CY helmet's XPF Auxetic Foam comfort pads. Further, the Soft Hydraulic Shocks demonstrated a contact pressure against the headform that was below a previously proposed threshold for football helmet discomfort [56]. At the unit level, we found that replacing existing comfort padding with the Soft Hydraulic Shock consistently improved the energy absorption ratio of the shock absorber-comfort pad system in not only the LS1-CY helmet, but also when replacing comfort padding from three other football helmets. Although these unit testing results are encouraging, full helmet tests would be required for the other three helmets (and any additional helmets) to confirm that the Soft Hydraulic Shock would improve safety performance as a comfort pad in each. As a second application of the Soft Hydraulic Shock in a football helmet, we integrated a single-stack Soft Hydraulic Shock into an existing helmet chinstrap. At a low impact velocity representative of repeated, subconcussive head impacts in youth football, the Soft Hydraulic Shock chinstrap dramatically reduced DAMAGE and HARM. At a higher velocity representative of youth football concussions, the chinstrap still afforded significant reductions in these injury risk metrics relative to the standard chinstrap. Although the clinical significance of the reductions in injury risk metrics observed in our full helmet tests is not entirely understood, integration of the Soft Hydraulic Shock into a comfort padding system or a chinstrap represents potentially meaningful applications for improving athlete brain safety. We find these applications especially encouraging from an industry perspective as they would not require as much design and development costs as would be needed to redesign the entire energy-absorbing liner of a helmet. Further, and most importantly, these results demonstrate the impressive ability of the Soft Hydraulic Shock to attenuate brain injury risk metrics even when only a small amount of the technology is implemented into a helmet system (e.g., one single-stack unit in the chinstrap). In the present study, we did not explore integrating the Soft Hydraulic Shock as the main energy-absorbing liner of a helmet, as significant design and engineering efforts would be required to ensure proper fit and sizing of the helmet. However, two previous studies utilizing FE modeling found that helmet safety metrics (e.g., HARM, head accelerations, and brain strain) could be improved by implementing liquid shock absorbers as the primary energy-absorbing structures in an American football helmet [68,69]. Therefore, as a next step towards evaluating the protective ability of liquid shock absorbers, we plan to develop and test a full helmet system with liquid shock absorbers as the primary energy-absorbing liner. Other than helmets, the Soft Hydraulic Shock can also be applied to other wearable PPE, such as knee pads or shoulder pads, which will be investigated in the future.

Although we demonstrated promising applications of the Soft Hydraulic Shock in a full helmet system, further research and development efforts would be necessary to successfully translate our prototypes into a safety product. Firstly, more testing would need to be performed to ensure that impact safety performance could be improved or maintained at more impact locations around the helmet and that the inclusion of the Soft Hydraulic Shock would not diminish impact attenuation anywhere in the helmet. The fit, comfort, and aesthetics of the technology would also need to be evaluated, ideally with human subjects, to verify that the device meets the standards of customers in the American football market or any other market where the device may be used. Finally, our study did not explore the failure limits of the Soft Hydraulic Shock. The upper limit of impact energy that the device can tolerate without permanent failure remains unknown, and a future study determining this limit and characterizing failure behavior, using either physical experiments or stochastic approaches based on FE modeling [70], would be necessary to demonstrate the device is suitable for PPE applications.

The present study has several limitations that are worth noting. The temperature tests in this study were performed in an ambient temperature environment. Though the shock absorbers were tested within 60 s of removal from the incubator or freezer, different heat capacities of the shock absorbers might have resulted in the shock absorbers being tested at different temperatures. A future comprehensive study about the effects of temperature on helmet shock absorber performance should be conducted with a temperature-controlled testing environment and more loading conditions. For the physical experiments, we focused on energy absorption ratio as the primary shock absorber performance metric and did not make comparisons of peak force or force efficiency. Peak force and force efficiency are metrics that are more sensitive to the impact loading conditions. The existing shock absorbers were extracted directly from helmets, so the impact loading for which each individual shock absorber was designed is unknown. In contrast, energy absorption ratio is a metric that mainly depends on the dissipation mechanism and is less influenced by impact loading. In the FE simulations, we applied the pressure that was calculated by the volume rate to the inner surface of the absorber, rather than modeling the fluid, orifice tube, and refill chamber [50]. In the actual refilling process, the elasticity of the refill chamber will yield back pressure to push the fluid back into the medical balloon to make the absorber ready for the next impact. Since the refill chamber was not modeled, this refilling process was not well captured in the simulation tests. Therefore, the small fluctuations in the force-displacement curves found in the physical experiments could not be observed in the FE simulations (Fig. 6), and the FE model was mainly used to investigate the compression phase instead of the rebound phase. The FE model was also not validated for the bottom-out scenario. Therefore, in the tests with the highest impact speed and heaviest mass, a small tail can be observed at the end of the impact in the physical experiments, but not in the FE model. Furthermore, the zero-strain state of the fabric in the physical prototype was in a flat form (Fig. 1d), while it was in a curved form (Fig. S2) in the FE model, which may have caused buckling and more self-contact between the fabric during compression. The FE model was also developed and validated solely for the ambient temperature condition in our study. Although the experimental impact response of the Soft Hydraulic Shock was relatively consistent across all three tested temperature conditions, further work would be necessary to assess which model parameters require changing to validate the model for the hot and cold temperature conditions.

5. Conclusions

In this study, we designed and prototyped the Soft Hydraulic Shock, a novel, compact, liquid-filled shock absorber that could be implemented into wearable PPE, such as helmets. In unit-level impact tests, the Soft Hydraulic Shock demonstrated superior performance compared to existing state-of-the-art compact shock absorbers, exhibiting an efficient dissipation of impact energy across a range of impact loading conditions and maintaining consistent performance across high, low, and ambient temperatures. The Soft Hydraulic Shock represents a major advance in shock absorber technology, eliminating the need for the heavy, rigid, metal structures typical of traditional hydraulic shock absorbers and thus enabling the ability for hydraulics to more easily be applied to PPE and other space-constrained applications.

Development and validation of a FE model of the Soft Hydraulic Shock enabled a platform for optimizing the design parameters of the device for improved force attenuation. FE model simulations revealed that orifice area and fabric longitudinal modulus were the most influential parameters in determining impact performance and elucidated a

critical orifice area for the device to yield minimized peak force for specified loading conditions. Optimized orifice area was found to vary primarily with impact mass, rather than impact speed, making the device a suitable candidate for PPE products for applications like contact sports, where impact speed can range considerably.

Finally, this study demonstrates the successful translation of the Soft Hydraulic Shock to a wearable PPE application. Laboratory headform impact testing supported two potential product embodiments for incorporation of the Soft Hydraulic Shock in a youth American football helmet that could lead to attenuated brain injury risk. To the best of the authors' knowledge, these results are the first published demonstration of a hydraulic shock absorber in a physical helmet. Overall, the high energy absorption ratio, temperature stability, and speed-adaptive characteristics of the Soft Hydraulic Shock make it a favorable mechanism for dissipating impact energy that could be applied towards PPE, including helmets.

CRediT authorship contribution statement

Nicholas J. Cecchi: Writing – review & editing, Writing – original draft, Validation, Methodology, Investigation, Formal analysis, Data curation, Conceptualization. **Yuzhe Liu:** Writing – review & editing, Writing – original draft, Validation, Methodology, Investigation, Formal analysis, Data curation, Conceptualization. **Ramanand V. Vegesna:** Writing – original draft, Methodology, Investigation, Formal analysis, Data curation. **Xianghao Zhan:** Methodology, Formal analysis. **Weiguang Yang:** Validation, Methodology, Formal analysis. **Leslie Anasu Espinoza Campomanes:** Investigation, Data curation. **Gerald A. Grant:** Writing – review & editing, Resources, Project administration, Funding acquisition. **David B. Camarillo:** Writing – review & editing, Resources, Project administration, Funding acquisition, Conceptualization.

Declaration of competing interest

The authors declare the following financial interests/personal relationships which may be considered as potential competing interests:

Nicholas Cecchi reports financial support was provided by the National Science Foundation. Gerald Grant, David Camarillo, Yuzhe Liu and Nicholas Cecchi reports financial support was provided by the Taube Stanford Concussion Collaborative. David Camarillo and Gerald Grant reports financial support was provided by the National Institutes of Health. Yuzhe Liu reports financial support was provided by the National Natural Science Foundation of China Young Scholar Program. Yuzhe Liu reports financial support was provided by the Young Elite Scientists Sponsorship Program by CSTAM. Yuzhe Liu reports financial support was provided by the Beihang University Frontier Multidisciplinary Program. David Camarillo reports a relationship with Savior Brain, Inc that includes: board membership, consulting, or advisory, equity or stocks. Gerald Grant reports a relationship with Savior Brain, Inc that includes: consulting or advisory and equity or stocks. David Camarillo has patent pending to Savior Brain, Inc and Stanford University. Nicholas Cecchi has patent pending to Savior Brain, Inc and Stanford University. The other authors declare that they have no known competing financial interests or personal relationships that could have appeared to influence the work reported in this paper.

Data availability

Data will be made available on request.

Acknowledgments

This study was supported by NIH Small Business Innovation Research (SBIR) grant R41 NS119134-01, the Taube Stanford Concussion Collaborative, a Graduate Research Fellowship from the National Science Foundation, National Natural Science Foundation of China Young Scholar Program 1230021530, Young Elite Scientists Sponsorship Program by CSTAM 2023-XSC-HW3, and the Fundamental Research Funds for the Central Universities YWF-23-Q-1029. The authors would like to thank LIGHT Helmets for providing the helmets used for testing in this study. Authors David Camarillo and Gerald Grant have a financial interest in Savior Brain, Inc., a company which has filed a patent application that claims the design of the novel shock absorber described in this work. David Camarillo and Nicholas Cecchi are listed as inventors on this patent application.

Supplementary materials

Supplementary material associated with this article can be found, in the online version, at doi:10.1016/j.ijmecsci.2024.109097.

References

[1] Sone JY, Kondziolka D, Huang JH, Samadani U. Helmet efficacy against concussion and traumatic brain injury: a review. J Neurosurg 2017;126:768–81.
[2] Yoganandan N, Pintar FA. Biomechanics of temporo-parietal skull fracture. Clin Biomech 2004;19:225–39.
[3] McAllister TW. Neurobiological consequences of traumatic brain injury. Dialogues Clin Neurosci 2011;13:287–300.
[4] James SL, et al. Global, regional, and national burden of traumatic brain injury and spinal cord injury, 1990–2016: a systematic analysis for the Global Burden of Disease Study 2016. Lancet Neurol 2019;18:56–87.
[5] Pankow MP, et al. Head games: a systematic review and meta-analysis examining concussion and head impact incidence rates, modifiable risk factors, and prevention strategies in youth tackle football. Sports Med 2022;52:1259–72.
[6] Baker CE, Yu X, Patel S, Ghajari M. A review of cyclist head injury, impact characteristics and the implications for helmet assessment methods. Ann Biomed Eng 2023;51:875–904.
[7] Hajiaghamemar M, Margulies SS. Multi-scale white matter tract embedded brain finite element model predicts the location of traumatic diffuse axonal injury. J Neurotrauma 2021;38:144–57.
[8] O'Keeffe E, et al. Dynamic blood–brain barrier regulation in mild traumatic brain injury. J Neurotrauma 2020;37:347–56.
[9] Zhan X, et al. Translational models of mild traumatic brain injury tissue biomechanics. Curr Opin Biomed Eng 2022;24:100422.
[10] Zhan X, et al. Predictive factors of kinematics in traumatic brain injury from head impacts based on statistical interpretation. Ann Biomed Eng 2021;49:2901–13.
[11] Zhan X, et al. Rapid estimation of entire brain strain using deep learning models. IEEE Trans Biomed Eng 2021;68:3424–34.
[12] Sabet AA, Christoforou E, Zatlin B, Genin GM, Bayly PV. Deformation of the human brain induced by mild angular head acceleration. J Biomech 2008;41:307–15.
[13] Fanton M, Kuo C, Sganga J, Hernandez F, Camarillo DB. Dependency of head impact rotation on head-neck positioning and soft tissue forces. IEEE Trans Biomed Eng 2018;66:988–99.
[14] Smith TA, et al. Angular head motion with and without head contact: implications for brain injury. Sports Eng 2015;18:165–75.
[15] Whyte T, et al. A review of impact testing methods for headgear in sports: considerations for improved prevention of head injury through research and standards. J Biomech Eng 2019;141:070803.
[16] Di Landro L, Sala G, Olivieri D. Deformation mechanisms and energy absorption of polystyrene foams for protective helmets. Polym Test 2002;21:217–28.
[17] Salimi Jazi M, Rezaei A, Karami G, Azarmi F, Ziejewski M. A computational study of influence of helmet padding materials on the human brain under ballistic impacts. Comput Methods Biomech Biomed Eng 2014;17:1368–82.
[18] Bhinder J, Verma SK, Agnihotri PK. Qualifying carbon nanotube reinforced polyurethane foam as helmet inner liner through *in-situ*, static and low velocity impact testing. Mater Sci Eng B 2021;274:115496.
[19] Leng B, Ruan D, Tse KM. Recent bicycle helmet designs and directions for future research: a comprehensive review from material and structural mechanics aspects. Int J Impact Eng 2022;168:104317.
[20] Nasim M, Hasan MJ, Galvanetto U. Impact behavior of energy absorbing helmet liners with PA12 lattice structures: a computational study. Int J Mech Sci 2022; 233:107673.
[21] Li S, Xiao Z, Zhang Y, Li Q. Impact analysis of a honeycomb-filled motorcycle helmet based on coupled head-helmet modelling. Int J Mech Sci 2021;199:106406.
[22] Adams R, Townsend S, Soe S, Theobald P. Finite element-based optimisation of an elastomeric honeycomb for impact mitigation in helmet liners. Int J Mech Sci 2022; 214:106920.
[23] Stewart D, Goel R, Christou G, Young L, Gilchrist M. Evaluating the performance of helmet linings incorporating fluid channels. J ASTM Int 2010;7:1–7.
[24] Cecchi NJ, et al. Identifying factors associated with head impact kinematics and brain strain in high school American football via instrumented mouthguards. Ann Biomed Eng 2021;49:2814–26.

[25] Giudice JS, et al. Finite element model of a deformable American football helmet under impact. Ann Biomed Eng 2020;48:1524–39.
[26] Decker W, et al. Development and multi-scale validation of a finite element football helmet model. Ann Biomed Eng 2020;48:258–70.
[27] Corrales M, et al. Validation of a football helmet finite element model and quantification of impact energy distribution. Ann Biomed Eng 2020;48:121–32.
[28] Bustamante M, et al. Component-level finite element model and validation for a modern American football helmet. J Dyn Behav Mater 2019;5:117–31.
[29] Post A, et al. Brain tissue analysis of impacts to American football helmets. Comput Methods Biomech Biomed Eng 2018;21:264–77.
[30] Ghazi K, Begonia M, Rowson S, Ji S. American football helmet effectiveness against a strain-based concussion mechanism. Ann Biomed Eng 2022;50:1498–509.
[31] Abayazid F, Ding K, Zimmerman K, Stigson H, Ghajari M. A new assessment of bicycle helmets: the brain injury mitigation effects of new technologies in oblique impacts. Ann Biomed Eng 2021;49:2716–33.
[32] Bailey AM, et al. Development and evaluation of a test method for assessing the performance of American football helmets. Ann Biomed Eng 2020;48:2566–79.
[33] Bland ML, McNally C, Zuby DS, Mueller BC, Rowson S. Development of the STAR evaluation system for assessing bicycle helmet protective performance. Ann Biomed Eng 2020;48:47–57.
[34] Rowson S, Duma SM. Development of the STAR evaluation system for football helmets: integrating player head impact exposure and risk of concussion. Ann Biomed Eng 2011;39:2130–40.
[35] Hui S, Yu T. Modelling of the effectiveness of bicycle helmets under impact. Int J Mech Sci 2002;44:1081–100.
[36] Rezayaraghi F, et al. Modal analysis of computational human brain dynamics during helmeted impacts. Brain Multiphys 2023;5:100082.
[37] Joodaki H, et al. Relative motion between the helmet and the head in football impact test. J Biomech Eng 2019;141:081006.
[38] Fahlstedt M, Halldin P, Kleiven S. The protective effect of a helmet in three bicycle accidents—A finite element study. Accid Anal Prev 2016;91:135–43.
[39] Cetin E, Baykasoğlu C. Energy absorption of thin-walled tubes enhanced by lattice structures. Int J Mech Sci 2019;157:471–84.
[40] Li W, Luo Y, Li M, Sun F, Fan H. A more weight-efficient hierarchical hexagonal multi-cell tubular absorber. Int J Mech Sci 2018;140:241–9.
[41] Zhu F, Dong L, Ma H, Chou CC, Yang KH. Parameterized optimal design of a novel cellular energy absorber. Int J Mech Sci 2014;86:60–8.
[42] Liu Y, Qiu X. A theoretical study of the expansion metal tubes. Int J Mech Sci 2016;114:157–65.
[43] Liu Y, Qiu X, Wang W, Yu T. An improved two-arcs deformational theoretical model of the expansion tubes. Int J Mech Sci 2017;133:240–50.
[44] Liu Y, Qiu X. A theoretical model of the shrinking metal tubes. Int J Mech Sci 2018;144:564–75.
[45] Liu Y, Qiu X, Yu T. A theoretical model of the inversion tube over a conical die. Thin Walled Struct 2018;127:31–9.
[46] Dixon JC. The shock absorber handbook. SAE International; 1999.
[47] Zhu X, Jing X, Cheng L. Magnetorheological fluid dampers: a review on structure design and analysis. J Intell Mater Syst Struct 2012;23:839–73.
[48] Clark D. Effects of repeated mild head impacts in contact sportsAbout concussion: adding it up. Neurology 2012;78:e140–2.
[49] Crisco JJ, et al. Frequency and location of head impact exposures in individual collegiate football players. J Athl Train 2010;45:549–59.
[50] Fanton M, et al. Variable area, constant force shock absorption motivated by traumatic brain injury prevention. Smart Mater Struct 2020;29:085023.
[51] Gabler LF, Crandall JR, Panzer MB. Development of a second-order system for rapid estimation of maximum brain strain. Ann Biomed Eng 2019;47:1971–81.
[52] Versace J. A review of the severity index. SAE Technical Paper 710881. 15th Stapp Car Crash Conference; 1971. p. 26. https://doi.org/10.4271/710881.
[53] Brahma I. Measurement and prediction of discharge coefficients in highly compressible pulsating flows to improve EGR flow estimation and modeling of engine flows. Front Mech Eng 2019;5:25.
[54] Almeida Jr JHS, Christoff BG, Tita V, St-Pierre L. A concurrent fibre orientation and topology optimisation framework for 3D-printed fibre-reinforced composites. Compos Sci Technol 2023;232:109872.
[55] Mortazavian S, Fatemi A. Effects of fiber orientation and anisotropy on tensile strength and elastic modulus of short fiber reinforced polymer composites. Compos Part B Eng 2015;72:116–29.
[56] Jadischke R, Viano DC, Dau N, King AI, McCarthy J. On the accuracy of the Head Impact Telemetry (HIT) System used in football helmets. J Biomech 2013;46:2310–5.
[57] Spelay RB, Adane KF, Sanders RS, Sumner RJ, Gillies RG. The effect of low Reynolds number flows on pitot tube measurements. Flow Meas Instrum 2015;45:247–54.
[58] Hansen K, et al. Angular impact mitigation system for bicycle helmets to reduce head acceleration and risk of traumatic brain injury. Accid Anal Prev 2013;59:109–17.
[59] Ramirez B, Misra U, Gupta V. Viscoelastic foam-filled lattice for high energy absorption. Mech Mater 2018;127:39–47.
[60] Cecchi NJ, et al. Padded helmet shell covers in American football: a comprehensive laboratory evaluation with preliminary on-field findings. Ann Biomed Eng 2023:1–14. https://doi.org/10.1007/s10439-023-03169-2.
[61] Rowson S, Duma SM. The temperature inside football helmets during head impact: a five-year study of collegiate football games. Proc Inst Mech Eng Part P J Sports Eng Technol 2013;227:12–9.
[62] Cecchi NJ, Oros TJ, Ringhofer JJ, Monroe DC. Comparison of head impact attenuation capabilities between a standard American football helmet and novel protective equipment that couples a helmet and shoulder pads. Sports Eng 2019;22:16.
[63] Gamble AS, et al. Helmet fit assessment and concussion risk in youth ice hockey players: a nested case-control study. J Athl Train 2021;56:845–50.
[64] Cecchi NJ, et al. The effectiveness of protective headgear in attenuating ball-to-forehead impacts in water polo. Front Sports Act Living 2019;2. https://doi.org/10.3389/fspor.2019.00002.
[65] Lu G, Yu T. Energy absorption of structures and materials. Elsevier; 2003.
[66] Finan JD, Nightingale RW, Myers BS. The influence of reduced friction on head injury metrics in helmeted head impacts. Traffic Inj Prev 2008;9:483–8.
[67] Zhan X, et al. The relationship between brain injury criteria and brain strain across different types of head impacts can be different. J R Soc Interface 2021;18:20210260.
[68] Cecchi NJ, Vahid Alizadeh H, Liu Y, Camarillo DB. Finite element evaluation of an American football helmet featuring liquid shock absorbers for protecting against concussive and subconcussive head impacts. Front Bioeng Biotechnol 2023;11:1160387.
[69] Vahid Alizadeh H, Fanton MG, Domel AG, Grant G, Camarillo DB. A computational study of liquid shock absorption for prevention of traumatic brain injury. J Biomech Eng 2021;143:041008.
[70] Lindberg G, Kulachenko A. Tray forming operation of paperboard: a case study using implicit finite element analysis. Packag Technol Sci 2022;35:183–98.